LBL-2270
c.1

THE ROLE OF DISLOCATION INTERACTION WITH SOLUTE ATOMS IN THE STRENGTHENING OF METALS

Chol Kyl Syn
(Ph. D. thesis)

November 1973

Prepared for the U. S. Atomic Energy Commission
under Contract W-7405-ENG-48

For Reference

Not to be taken from this room

RECEIVED
LAWRENCE
RADIATION LABORATORY

JAN 2 1974

LIBRARY AND
DOCUMENTS SECTION

LAWRENCE BERKELEY LABORATORY
UNIVERSITY OF CALIFORNIA
BERKELEY

LBL-2270
c.1

DISCLAIMER

This document was prepared as an account of work sponsored by the United States Government. While this document is believed to contain correct information, neither the United States Government nor any agency thereof, nor the Regents of the University of California, nor any of their employees, makes any warranty, express or implied, or assumes any legal responsibility for the accuracy, completeness, or usefulness of any information, apparatus, product, or process disclosed, or represents that its use would not infringe privately owned rights. Reference herein to any specific commercial product, process, or service by its trade name, trademark, manufacturer, or otherwise, does not necessarily constitute or imply its endorsement, recommendation, or favoring by the United States Government or any agency thereof, or the Regents of the University of California. The views and opinions of authors expressed herein do not necessarily state or reflect those of the United States Government or any agency thereof or the Regents of the University of California.

THE ROLE OF DISLOCATION INTERACTION WITH SOLUTE ATOMS IN THE STRENGTHENING OF METALS

Contents

ABSTRACT v

GENERAL INTRODUCTION 1

PRELIMINARY REVIEW 4

PART 1. INTERACTIONS BETWEEN AN EDGE DISLOCATION AND AND SUBSTITUTIONAL SOLUTE ATOMS IN AN ANISOTROPIC HCP CRYSTAL 8

I. Introduction 8

II. Formulation and Computation of the Interaction Energy . . . 10

A. The "Size" Effect 10

B. The "Modulus" Effect 11

C. Computation 12

III. Force-Displacement Relation 13

VI. Discussion 16

A. Effect of Anisotropy 16

B. Core Correction 20

C. Core Solute Atoms 20

D. Effect of Annealing Temperature 24

V. Conclusions 25

PART 2. EQUILIBRIUM CONFIGURATION OF DISLOCATION IN THE STRAIN FIELD OF SUBSTITUTIONAL SOLUTE ATOMS 26

I. Introduction 26

II. Summary of the Existing Theories 28

A. Theory of Mott and Friedel 28

B. Friedel's Forest Model 29

C. Fleischer's Theory 31

III. Formulation 33

IV. Computation and Results 37

A. Computation Algorithm 37

B. Results for Alternating Arrays 37

C. Dislocation Configurations and Flow Stresses in Unmixed Arrays 39

V. Point Obstacle Approximation 42

VI. Discussion 47

A. Relevance of Assumptions 47

B. Strengths of Repulsive and Attractive Arrays 48

C. Point-Obstacle Approximation 50

D. Perturbation of Dislocation Configuration 52

VII. Conclusions 55

ACKNOWLEDGMENTS 56

APPENDIX: Estimation of Elastic Constants of FCC Element in HCP Structure 57

REFERENCES 59

FIGURE CAPTIONS 63

THE ROLE OF DISLOCATION INTERACTION WITH SOLUTE ATOMS IN THE STRENGTHENING OF METALS

Chol Kyl Syn

Inorganic Materials Research Division, Lawrence Berkeley Laboratory and Department of Materials Science and Engineering, College of Engineering; University of California, Berkeley, California

ABSTRACT

In Part 1, the anisotropic elastic interaction energy of a straight edge dislocation with a substitutional solute atom of Ag or Cd in the matrix of Zn is computed. Then the force-displacement relation for rigid glide of the dislocation with respect to the solute atmosphere is calculated. It is shown that the anisotropic elasticity can reveal some important details which are not found in the isotropic elasticity approach, and that different sources of interaction contribute additively to the total interaction energy, but non-additively to the total force for the rigid glide. A detailed discussion indicates that solute atoms within the dislocation core may not distribute uniformly along the dislocation line, but form discrete clusters.

In Part 2, the equilibrium configurations of dislocation lines in the shear stress fields of substitutional solute atoms distributed in square arrays and the flow stresses required to drive the dislocation lines through such arrays are computed by numerical methods and then compared with the predictions by the theories on the dislocation-point obstacle interaction. The assumptions used in the point-obstacle approximation is shown to be justifiable to a considerable accuracy. An

attractive solute atom turns out to be a stronger obstacle than a repulsive one and it is attributed to the fact that the attractive solute atom faces the dislocation on the steeper side of its shear stress field while the repulsive solute does so on the other side.

GENERAL INTRODUCTION

Theoretical considerations on the stress to initiate dislocation glides through obstacles in metallic crystals of dilute binary solid solution at low temperatures can be categorized in two groups. The first group[1-3] is concerned with the stress needed to free a dislocation from the cloud of solute atoms which are segregated at and around the dislocation itself. The second group[4,5] treats the computation of the stress required to move a dislocation through discrete solute atoms which are uniformly distributed at random on the dislocation glide plane. The second group includes what are customarily known as theories on "solution hardening"; the first group includes theories usually referred to as the "Cottrell-Bilby" theory or "locking" theories. The initial stress is commonly referred to as "yield stress" in the "locking" theories because the liberation of the locked dislocation from the solute cloud is predicted to involve a distinctive yield point phenomenon. In the solution hardening theories the initial stress is referred to as the "flow stress" since it is not predicted to show yield point pheonomenon and is simply the beginning of plastic flow.

The appearance of an abrupt maximum in the tensile stress-strain curve at the onset of a large-scale plastic flow is known as the yield point phenomenon. Johnston and Gilman[6] have proposed a different interpretation of this phenomenon. From experimental observation, they attribute the sharp drop in stress to the rapid generation of large number of mobile dislocations. Thus it seems that the solute atom locking of dislocation does not have to be invoked to explain the

the yield point phenomena in general. As for the "solution hardening", some of earlier well-designed experimental observations[10-13] indicated that solution hardening comes from the increased density of grown-in dislocations upon alloying. However recent experiments,[14] which were done with Cu crystals with very low initial dislocation density ($< 10^4/cm^2$), show that the flow stress is independent of the initial dislocation density.

The "locking" concept seems to be rather well established. It is a very useful concept in the "serrated yielding", which is a repeated appearance of yield point phenomena over a certain range of temperature and strain rate during plastic flow in commercially pure or dilutely alloyed metals.[15] However, all of the "locking" theories allow the dislocation core (the region within one Burgers vector range) to be saturated with solute atoms. Thus the solute concentration within the core becomes much higher than the solubility limit. Nevertheless, no considerations are given to this aspect in the theories. In the "solution hardening", it is conceivable that the interaction between the gliding dislocation and individual solute atoms is more important than the interaction between dislocations, at least in crystals with low dislocation density. However, most of the theories fail to recognize the fact that exactly half of the randomly distributed solute atoms on any glide plane in a crystal of binary solid solution are attractive obstacles to dislocations, while the other half are repulsive, if only the "size" effect is considered. One other important problem is the general tendency to regard the solute atoms as point obstacles, since it simplifies the computer simulations[16-18] of dislocation movement

through the randomly distributed solute atoms. This assumption also enables the statistical treatments[19-22] of the same problem in simple forms.

It is therefore important to re-examine closely the above-described problems and clarify the confusing points. Rather than to propose a complete new theory, however, it would be more worthwhile to look into the basic assumptions and concepts from different viewpoints from those of the existing theories. By removing some of the assumptions, adding some other new ones, and applying some more realistic computing devices, we may be able to extract a few useful and important conclusions. To this end, we divide this paper into two parts. In Part 1, we will examine and discuss the "locking" phenomenon more in detail. In Part 2, we will investigate the solute-dislocation interaction without introducing some of the assumptions used in other theories and clarify the limit of the "point-obstacle" approximation. The scope of the problems and the main assumptions used will be described in the introduction section in each part and the discussions will be done separately in each part.

Before we start Part 1, we will review rather in detail the interaction between a substitutional solute atom and an edge dislocation due to the "size" effect. This is known as the most dominant source of the interaction in most of the common solid solutions.

PRELIMINARY REVIEW

Usually the solute atom-dislocation interaction is analyzed in terms of linear isotropic elasticity. A spherical cavity of radius r_o is cut in an elastic continuum of the matrix[22]; an elastic sphere of radius r', representing the solute atom, is introduced and the are pulled together and cemented at an equilibrium radius $r = r_o(1+\varepsilon)$, where ε is the atomic size misfit (an experimental measure of ε is given by $1/a \cdot da/dc$ [23] where a is the lattice parameter and c is the solute concentration of solute). Since a spherical inclusion causes radial displacements only, the elastic strain field of the solute atom interacts with the hydrostatic component of the dislocation stress field. The elastic work done in this interaction gives the interaction energy due to the "size effect".

In the linear elastic approximation a pure screw dislocation has no hydrostatic stress component and spherical solute atoms interact only with the edge components of dislocations. There is nevertheless an elastic interaction between a substitutional solute atom and a screw dislocation.[24] It results from the torque that the stress field of the solute atom exerts on the dislocation, trying to twist it into an edge orientation where the strain energy interaction can lower its total energy.

For our purpose in Part 2, it will be more convenient to represent the elastic distortions due to solute atoms by internal back stresses on the glide plane. In Fig. 1, the x-y plane is the glide plane of an edge dislocation with Burgers vector b in the y-direction and a solute

atom is located at (o,o,h). Then as shown by Weertman and Weertman,[25] the solute atom causes a shear stress in the glide plane, in the direction of b, equal to

$$\tau_{zy} = 6G\, r_o^3\, \varepsilon\, \frac{yh}{(x^2+y^2+h^2)^{5/2}} \tag{1}$$

where G is the shear modulus. The elastic constants of solvent and solute are assumed to be identical in deriving Eq. (1). If we select the (111) plane as the glide plane in fcc crystals, we obtain $h_1 = \pm b/\sqrt{6}$ for solute atoms on the nearest atomic layers to the glide plane, and $h_2 = \pm 3b/\sqrt{6}$ for second layer solute atoms. It is clear from Eq. (1) that the solute atom at (x,y,h) exerts a back stress to the dislocation which is exactly opposite to the back stress due to the solute atom at (x,y,-h).

The interaction energy, U, between an infinitely long edge dislocation and an individual solute atom is obtained by the integration of τ_{zy} as follows

$$U = \int_{-\infty}^{y}\int_{-\infty}^{\infty} \tau_{zy}\, b\, dxdy \tag{2}$$

which, when integrated, gives the well known Cottrell interaction energy,[21]

$$U = 4\, G\, r_o^{\,3}\, \varepsilon\, b\, \frac{h}{y^2+h^2} \tag{2b}$$

The force-displacement relationship for cutting the stress field of an isolated solute atom by a long, straight edge dislocation, is obtained by taking the derivative of U with respect to y:

$$F = -\partial U/\partial y = -8\,G\varepsilon\, r_o^{\,3} b \;\frac{yh}{(y^2+h^2)^2} \tag{3}$$

Cottrell[26] has pointed out that Eq. (2b) overestimates the interaction energy near the center of the dislocation because of the effects of core and deviations from Hooke's law. He has suggested that these effects can be taken into account approximately by altering Eq. (2b) to

$$U = 4\,G\varepsilon\, r_o^{\,3}\, b \;\frac{h}{y^2+h^2+\rho^2} \tag{4}$$

where ρ can be thought of as the effective width of the dislocation. At dislocation-solute spacings less than ρ, the only interaction is with the crystal itself and not with the dislocation. The corresponding force-displacement relation becomes

$$F = -8\,G\, r_o^{\,3}\, \varepsilon\, b \;\frac{yh}{(y^2+h^2+\rho^2)^2} \tag{5}$$

Stefansky and Dorn[27] adopt a new correction term $f = 1-\exp\{-\beta(x^2+y^2+h^2)/b^2\}$ which is a mathematical equivalent to the Cottrell's correction, such that

$$-\int_{-\infty}^{y}\int_{-\infty}^{\infty} \tau_{zy} b f dx dy = 4\,G r_o^{\,3}\,\varepsilon b \;\frac{h}{y^2+h^2+\rho^2} \tag{6}$$

In Eq. (6), the corrected total work done by τ_{yz}, is equated to the corrected interaction energy of Cottrell's. These corrections are significant only within the dislocation core region of one Burgers vector from

the disloction center, and are imperceptibly small outside the core region.

The common practices have been to leave this core region out of the analysis, because of the breakdown of the linear elasticity. However, the most significant part of the interaction can occur within the core. Since no other simple, usable alternative ways are available, it seems, to be rather profitable to employ the core corrections, even if the validity of the corrections is open to a serious debate. In principle, the correction factors ρ or β can be determined by comparing measured binding energies for substitutional solute atoms with the predictions of Eq. (4). The results, however, are not convincing, since it is difficult to estimate the elastic contribution to the measured energies. We will employ the correction term of Stefansky and Dorn, because it is more convenient to use in the numerical computations. We will uniformly set $\beta = 3$, which is equivalent to $\rho^2 = 0.07\ b^2$, following Stefansky and Dorn.[27]

PART 1. INTERACTIONS BETWEEN AN EDGE DISLOCATION AND SUBSTITUTIONAL SOLUTE ATOMS IN AN ANISOTROPIC HCP CRYSTAL

I. INTRODUCTION

In this part, we will investigate the interaction of a straight edge dislocation with substitutional solute atoms which are locally concentrated about the dislocation. By using the core correction of Stefansky and Dorn, and by following the "locking" theory of Jacobson,[3] we will evaluate the interaction energy, force-displacement relation and solute concentration within and around the dislocation core. Instead of the conventional practice of isotropic elasticity, we will employ the anisotropic elastic solution of the dislocation theory, because the letter is considered to give a more realistic result than the former. For a particular case of study, we have chosen Zn as the host metal and Ag and Cd as the solute species. The anisotropic elastic solution of the dislocation stress in HCP crystals is available in a simpler form than in other crystal structures. Zinc, with a non-ideal axial ratio of 1.85 shows a strong anisotropy in its elastic property and its elastic constants from 0°K to the melting point are known. Silver and cadmium distort the lattice of Zn in a contrasting way (see Discussion).

The investigation takes account for the anistropy under three approximations. First, the dislocation-solute interaction is assumed due to the elastic "size" and "modulus" effects. We neglect other sources of interaction.[5] Second, the solute concentration in the bulk is so small that the solid solution is assumed to be an ideal solution. We neglect chemical and elastic solute-solute interactions.

Third, the breakdown of linear elasticity within the dislocation core is artificially removed by following the Stefansky-Dorn method described in the preliminary review.

In section II the anisotropic dislocation-solute interaction will be formulated and computed. Then the force-displacement relation governing rigid glide of an isolated dislocation will be computed with and without the artificial core correction in section III. In section IV, we will discuss the assumptions and results obtained in sections II and III, and the distribution of solute atoms within the dislocation core.

II. FORMULATION AND COMPUTATION OF THE INTERACTION ENERGY

A. The "Size" Effect

When a solute atom is substituted for a host atom in an anisotropic matrix containing an edge dislocation, the matrix is anisotropically strained against the dislocation stress field. If $\underset{\sim}{\varepsilon}$ is the tensor strain produced by the solute atom and $\underset{\sim}{\sigma}$ is the local tensor stress due to the dislocation, then the interaction energy, U_S°, is[28]

$$U_S^\circ = -\sum_{i,j} \sigma_{ij}\varepsilon_{ij}\Omega, \quad (i,j = x,y,z) \tag{7}$$

where Ω is the atomic volume of the matrix atoms.

In the coordinate system shown in Fig. 2, an edge dislocation on the basal plane lies parallel to $[10\bar{1}0]$, and its Burgers vector is parallel to $[\bar{1}2\bar{1}0]$. For this orientation the principal axes of the strain induced by a substitutional solute atom are parallel to the principal axes of the dislocation stress field. Hence Eq. (7) is reduced to

$$U_S^\circ = \sum_{i=1}^{3} \sigma_{ii}\varepsilon_{ii}\Omega = -\Omega(\varepsilon_{xx}\sigma_{xx}+\varepsilon_{yy}\sigma_{yy}+\varepsilon_{zz}\sigma_{zz}) \tag{8}$$

where the σ_{ii}'s are given by Chou,[29] and $\Omega = a^2c\sqrt{3/4}$ for the hcp crystal with lattice parameters a and c. The principal strains ε_{xx}, $\varepsilon_{yy}(=\varepsilon_{xx})$, and ε_{zz} can be estimated from the lattice parameter variation with average solute concentration C_o through the relation $\varepsilon_{zz} = 1/c\cdot dc/dC_o$ and $\varepsilon_{yy} = 1/a\cdot da/dC_o$.[23]

B. The "Modulus" Effect

If a substitutional solute atom has different elastic constants from those of the matrix, its elastic response to the dislocation stress field will be different from that of the matrix. Then the interaction energy, U_M^o, will be determined by computing the difference between the strain energy stored within the solute atom and the strain energy stored within an equal volume of the matrix, as follows[4]

$$U_M^o = \frac{1}{2}\int(\sigma'_{ij}e'_{ij} - \sigma_{ij}e_{ij})\,dv, \quad (i,j = x,y,z) \tag{9}$$

where σ'_{ij} and σ_{ij} are respectively the stresses acting on the solute and matrix, and e'_{ij} and e_{ij} are respectively the strain induced in the solute and the same volume of the matrix. The integration should be performed over the volume of the solute atom. If e'_{ij} is uniform within the solute atom and is the same as e_{ij}, we will have the following expression.

$$U_M^o = \frac{1}{2}\int(c'_{ijk\ell}e'_{ij}e'_{k\ell} - e_{ijk\ell}e_{ij}e_{k\ell})\,dv$$

$$= \frac{1}{2}\,\Omega\,(c'_{ijk\ell} - c_{ijh\ell})e_{ij}e_{k\ell}$$

$$= \frac{1}{2}\,\Omega\,\Delta\,c_{ijk\ell}e_{ij}e_{k\ell}, \quad (i,j = x,y,z) \tag{10}$$

where $c_{ijk\ell}$ and $c'_{ijk\ell}$ are respectively the elastic constants of the solute and the matrix. If the variation of the elastic constants with respect to the solute concentration C_o is known, then $\Delta c_{ijk\ell}$'s can be

replaced by $1/c_{ijk\ell}\ dc_{ijk\ell}/dC_o$ as Fleischer[30] does in analogy with the "size" effect. In most cases this variation is not known. As a crude approximation, we simply take the differences in the elastic constants of the metals of solute and matrix.

For solute elements of HCP structure, the five independent elastic constants are known and so are the five independent $\Delta c_{ijk\ell}$'s. For solute elements of FCC structure, we have to determine the five elastic constants for an imaginary HCP structure. For practical purposes, however, from the equivalence of atomic arrangement of (111) plane of FCC and (0001) plane of HCP, we can obtain the necessary elastic constants as is shown in Appendix.

C. Computation

The interaction energies, U_S° and U_M°, were computed for Ag and Cd solute atoms about an edge dislocation in Zn, oriented as in Fig. 2. The principal strains are $\varepsilon_{xx} = \varepsilon_{yy} = 0.35$ and $\varepsilon_{zz} = -0.71$ for Ag, $\varepsilon_{xx} = \varepsilon_{yy} = 0.11$ and $\varepsilon_{zz} = 0.27$ for Cd, computed from room temperature X-ray data.[31] The elastic constants of Zn,[32] Ag,[33] and Cd[34] at 300°K and 473°K were used in Eqs. (9) and (10). The computed contours of U_S°, U_M° and $U_S^\circ + U_M^\circ$ are plotted in solid lines (473°K) and dashed lines (300°K) in Figs. 3 to 5. Contours in dotted lines represent the isotropic interaction energies at 300°K. The numbers attached to the contours represent the interaction energy in units of eV.

III. FORCE-DISPLACEMENT RELATION

The force for an isolated edge dislocation to glide as a whole with respect to a single immobile atom is obtained from the following relation.

$$F = -\partial U_I/\partial y \tag{11}$$

where U_I represents the appropriate interaction energy. Then the total force due to the whole solute atmosphere will be obtained as a sum of the contributions from each solute atom in the atmosphere.

At a sufficiently high temperature, T_a, where diffusion can readily occur, the solute atoms will form an atmosphere about the isolated dislocation according to the following equilibrium relation.[5]

$$C_A(y,z) = \frac{C_o \exp[-U_I(y,z)/kT_a]}{1 - C_o + C_o \exp[-U_I(y,z)/kT_a]} \tag{12}$$

where k is the Boltzman factor, C_o the average atomic fraction of solute atoms in the matrix, and C_A the solute atom fraction at (y,z). If our specimen is annealed at T_a long enough for solute atoms to attain an equilibrium distribution given by Eq. (12), and then quenched rapidly enough to prevent subsequent diffusion, the solute atmosphere given by Eq. (12) will be retained and the dislocation will be locked by the solute atmosphere.

The force, F_I, per unit length of the dislocation resulting from the rigid displacement of the dislocation to a position, y', with respect to the immobile solute atmosphere will be[3]

$$F_I(y') = \sum_{y,z=-\infty}^{\infty} F(y') \frac{C_A(y,z)}{\Omega} \cdot \Delta V \tag{13}$$

where $F(y') = -\frac{\partial U_I(y-y',z)}{\partial y}$ is the force exerted on the dislocation at y' from a solute atom located at (y,z), C_A/Ω the volume fraction of solute atom at (y,z), and $\Delta V = 1 \cdot b \cdot c/2 = ac/2$ the elemental volume of an HCP crystal per unit length over which the solute atoms are distributed. The resolved shear stress, τ_I, on the glide plane in the direction of the Burgers vector (or y-direction) can be computed from the following relation

$$\tau_I(y')b = F_I(y') = \sum_y \sum_z -\frac{\partial U_I(y')}{\partial y} \frac{C_A(y,z)}{\Omega} \Delta V \qquad (14)$$

To introduce the core correction into the computation of τ_I, we have to multiply U_S° and U_M° in Sec. II by the correction term $f = 1-\exp[-\beta(x^2+y^2+z^2)/b^2]$, which was discussed in the preliminary review. Then U_I in Eq. (11) will represent the core-corrected interaction energy. Since our dislocation is straight and parallel to the x-axis and the matrix is an anisotropic HCP crystal, we used the correction term in the form of $f = 1-\exp[-3\{(y/a)^2+(z/c/2)^2\}]$ in the actual calculation.

The summation in Eq. (14) was done from -10 to +10 lattice sites for both y and z in the machine computation, for the forces beyond the limit are several orders of magnitude lower than the maximum force. The specimen was assumed to have been rapidly quenched to 0°K after annealing at 473°K, and then tested at 300°K. Therefore the elastic constants of Zn,[32] Ag[33] and Cd[34] at 473°K and 300°K were used to compute C_A and $\partial U_I/\partial y$ respectively.

Figures 6 and 7 show the results obtained from Eq. (14) for an

extremely dilute concentration, $C_o = 10^{-7}$. τ^S and τ^T (in solid lines) represent respectively the stresses due to "size" and "size + modulus" effects. τ_c^T (in dash-and-dotted lines) represents τ^T with the core correction. The stress due to only the "modulus" effect was computed and it turned out to be several orders of magnitude smaller than the stress due to the "size" effect. However, the difference between τ^S and τ^T tells us that the "modulus" effect may not be neglected at all. We will return to this point in the discussion section.

Other computations were done to see how much the solute atoms within the dislocation core contribute to the stress-displacement relations. It was found that more than 90% of the total force is contributed from the core solute atoms, as are shown in the dashed lines in Figs. 6 and 7.

VI. DISCUSSION

In this section, we will focus our discussion on the effects of the anisotropy, and effect of solute atoms and their distribution within the dislocation core to the solute-dislocation interaction. The core correction will be briefly discussed and its effect on the solute concentration will be incorporated in the effect of core solute atoms. The annealing or equilibrating temperature of the solute atmosphere will be briefly mentioned at the end of this section.

A. Effect of Anisotropy

1. Contrast in Energy Contours

Isotropic interaction energies at 300°K by "size" and "modulus" (shear modulus + bulk modulus) effects were computed from the expressions formulated by Cottrell and Bilby,[1] and Fleischer,[30] respectively, and plotted in dotted lines in Figs. 3 and 4 for comparison. We can see strong contrasts between the isotropic and anisotropic, and between Ag and Cd. The anisotropic interaction energies are of longer range and their contours are not circular. The anisotropic contours from the "size" effect interaction for Ag split into four leaves, while those for Cd are rather similar to the isotropic contours in shape. This strong contrast due to the "size" effect may be explained by the fact that Ag solute atoms expand the lattice along the a-axis and shrink it along the c-axis, while Cd solute atoms expand it in both directions, even though the expansion by Cd is highly anisotropic.

Two other interesting points emerge from the computation of the "size" contours. One point is the relative magnitude of the binding energy (at room temperature) in the conventional concept (i.e., the

maximum interaction energy at r =b). The conventional isotropic computation predicts 0.16 eV and 0.22 eV for Ag and Cd,[35] respectively, while the present computation shows that they are 0.37 eV and 0.39 eV, respectively. The other point is the position of the binding energy (or the maximum interaction energy on the circle of r = b). The conventional isotropic computation indicates that this position should be always one Burgers below the dislocation center (i.e. y = 0 and z = -b in the present coordinate system) if an oversized solute atom is involved. The present anisotropic approach shows that for Cd, the position is the same as predicted by the isotropic computation, but for Ag, it is different. As is clear from Fig. 3(a), for Ag, on the circle of r = b, there are two points at which the interaction energy becomes maximum. If the present computation is valid even within this circle we can also determine the lattice sites where the interaction energy becomes maximum. Since the nearest atomic layer below the dislocation is one half of d (= inter-planar spacing of atomic layers parallel to the dislocation glide plane =0.928b in Zn) away from the dislocation for Cd, (0,-d/2) is the site, and for Ag (-b,-d/2) and (+b,-d/2) are the sites. Actually, we have taken these sites as the dislocation core sites in the computation of solute concentration within the core.

The "modulus" contours at 473°K are of considerably longer range than those at 300°K, contrary to the case of the "size" contours. This seems to be caused by the faster decrease of the elastic constants of Zn than those of Ag and Cd as the temperature goes up, as is clear from Eq. (10).

The total "size and modulus" interaction contours, when compared with the "size" contours, are severely distorted within one half of a

Burgers vector, but are not perturbed seriously beyond that range. This is due to the fact that the "size" effect is of a longer range ($\sim 1/r$ dependence, where r is distance from the disloction center) than the "modulus" effect ($\sim 1/r^2$ dependence).

2. Force-Displacement Relation

The force-displacement diagrams by the "size" effect in Figs. 6 and 7 also show a strong contrast in shape between Ag and Cd. This is due to the difference in the shape of the interaction energy contours. For Ag, there are two potential-well like valleys below the dislocation [see Fig. 3(a)]. Thus every Ag solute atoms should climb up the steep potential slope twice, while each Cd solute atom should do so only once [see Fig. 3(b)]. This will be clearly understood if we move the solute atmosphere with respect to the dislocation instead of moving the dislocation with respect to the solute atmosphere.

As we briefly mentioned in Sec. III, the maximum stresses due to the "modulus" effect only turned out to be several orders of magnitude smaller than those due to the "size" effect. As is clear from Figs. 4(a) and (b), the "modulus" effect is locally concentrated around the dislocation center and the magnitude of interaction energy along the line, $z = -d/2$, will be small, compared with that of the "size" effect. However, when combined with the "size" effect, the "modulus" effect dramatically changes the force-displacement diagrams, at least in the present two cases. For Ag solute atoms, the "modulus" contours at 473°K with (+) sign stretched vertically over a rather long range, while the "size" contours of (-) sign extends in the directions tilted about 45° from the y-axis. When the two effects are combined, the

slope of the interaction potential (i.e. $\partial U_I/\partial y$ in Eq. 14) will sharply increase. The sign alternation of the "modulus" effect for Ag, at 473°K slightly increases the magnitude of the total interaction energy at the positions where the magnitude of the "size" interaction energy is maximum. Thus the combined interactions increase the maximum stress in the force-displacement diagram by a large amount. For Cd, the "modulus" interaction energy of (-) sign contributes to the total interaction energy by an amount which cannot be neglected, and which in turn exponentially increases the solute concentration, leading to the sharply heightened maximum of the force-displacement diagram. However, the negative "modulus" effect for Cd slightly decreases the slope of the interaction potential. Actually, when C_o is rather high ($> \sim 10^{-4}$), and hence the dislocation core is completely saturated with solute atoms at the same T_a = 473°K, we can show that the maximum stress in the force-displacement diagram due to the "size + modulus" effect is lower than that due to the "size" only.

From the discussion on the interaction energy contours and force-displacement diagram, we can conclude that if we use the isotropic approach to highly anisotropic crystals, we will certainly lose some very important details. Furthermore, we may not consider only one source of interaction, only because it is dominant, unless the interaction energy of this source is at least larger by one order of magnitude than the interaction energies due to other sources.

B. Core Correction

So far there is no way to estimate the correction factor, β precisely on a purely theoretical basis. The value of β would remain uncertain as is the whole experimental data on the binding energies, until more reliable experimental and theoretical developments are available. One promising approach seems to be the application of suitable interatomic potential to the discreet atomic lattices containing dislocations and vacancies.[36] But this approach is not developed enough yet to be applicable to the substitutional solute atom problem.

The core correction is more effective for Cd than for Ag. The correction term $f = 1 - \exp\{-3[(y/b)^2+(z/c/2)^2]\}$ actually reduces the interaction energy at $(y = 0, z = -b/2)$ about 50%. As a solute atom approaches closer to the dislocation center, the reduction of the interaction energy becomes larger. The lattice site of the maximum interaction energy for Cd is closer to the dislocation center than that for Ag, as is clear from Figs. 5(a) and (b).

C. Core Solute Atoms

As mentioned earlier, the dominant contribution to the force-displacement relation comes from the solute atoms within the dislocation core. This is due to a combination of the following two factors. First, the gradient of the interaction potential (i.e. $\partial U_I/\partial y$) is extremely steep within the core range. Second, the solute concentration within the core is also extremely high. Thus it is worthwhile to discuss the factors which affect the core concentration.

The core correction is an artificial device to remove the singularity of the linear elasticity which does not exist in the real crystals

containing dislocations and solute atoms. Thus the core concentration can be reduced by the core correction which in fact reduces the magnitude of the interaction energy within the core. The core concentration can be affected by the interactions between solute atoms themselves. Even though we stated that we neglect the chemical and elastic interaction between solute atoms, it seems very appropriate to check how these interactions can influence the core concentration. We consider three sources of solute-solute interaction, one direct and two indirect, as follows.

1. Direct Chemical Interaction

The solubilities of Ag and Cd in Zn are very small, which indicates there is a strong attractive interaction either between solute atoms or between solute and matrix atoms. Within the core crowded with solute atoms attractive to each other, the clustering of solute atoms is likely to occur. This attractive interaction between solute atoms will enhance the solute atom flow to the dislocation during the annealing at a high temperature, thus resulting in increasing the core concentration. On the other hand, the repulsion between solute atom would reduce the core concentration. Within the core, the repulsion would tend to prevent the clustering. But this repulsion will be blocked by the vibrational entropy effect which will be discussed later.

2. Relaxation Effect

The first group of solute atoms which arrived within the dislocation core during the annealing treatment would relax and somewhat neutralize the strain field of the dislocation. The relaxed dislocation then would exert a weaker attraction to the next group of solute atoms.

Thus the actual core concentration would be lower than that given by Eq. (12). This relaxation effect has been treated by Larché and Cahn[37]; a detailed discussion of which is beyond the scope of this paper.

3. Vibrational Entropy Effect[38,39]

Consider the solute atoms as pinning points and the dislocation as a vibrating string between the pinning points. The dislocation would tend to repel the solute atoms or push them into clusters to preserve its vibration frequency as low as possible, because the lower frequency is related to higher entropy. Considering this effect, Bauer[38] derived the following expression,

$$C_{co} = \frac{C_o \exp[-(U_c - \frac{1}{2} kT \ln C_{co})/kT_a]}{1-C_o+C_o \exp[-(U_c - \frac{1}{2} kT C_{co})/kT_a]} \tag{15}$$

where U_c is the interaction between the dislocation and solute atom within the core, and C_{co} is the core solute concentration. When $C_o << 1$, Eq. (15) is reduced to

$$C_{co} = C_o^2 \exp[-2U_c/kT_a] \tag{16}$$

Unless U_c is extremely large in magnitude, Eq. (16) leads to a tremendous reduction of the core concentration as shown below.

To see the effect of the core and Bauer corrections, we computed the core concentrations, i) without any correction, ii) with only core correction, and iii) with both corrections, as a function of C_o. The results are shown in Figs. 8 and 9. For Ag, the correction effects are negligible, when $C_o > 10^{-4}$, while for Cd, the core correction reduces significantly C_{co} even when $C_o > 10^{-4}$. The Bauer correction when

combined with the core correction causes an enormous reduction of C_{co} for Cd when $C_o < 10^{-4}$, and for Ag when $C_o < 10^{-5}$.

The theoretical development of the vibrational entropy effect is based on assumptions which are not compatible with those of the present paper. The expression of the vibrational entropy change of the dislocation due to solute atoms[38] approaches infinity as C_{co} decreases. Thus the correction effect becomes greater as the average concentration C_o decreases as is shown in Figs. 8 and 9. Nevertheless the concept of vibrational entropy implies an important consequence of clustering[39] of solute atoms which may or may not interact directly with each other. Thus if the solute concentration is higher than the solubility limit, the clustering will enhance the nucleation of second phase particles on the dislocation. There is no definite evidence yet to show the clustering of substitutional solute atoms in the dilute alloys. But Thompson[40] has provided evidence indicating the clustering of point defects (radiation-induced interstitials or vacancies) in irradiated Cu crystals when dislocations are saturated with such defects.

In terms of the clustering, the "locking" theories may have to be rephrased in the following framework. The solute atoms which are locking dislocations form clusters along the dislocations. When an external stress is applied, dislocations will bow out between clusters. The yield stress will be determined by the distribution of clusters and cluster strengths. Thus the force-displacement relation should be computed for the interaction between a flexible dislocation and a cluster.

D. Effect of Annealing Temperature

In the computation of the force-displacement relation, we considered only one annealing temperature, 473°K (~ 0.68 T_m. T_m = 693°K for Zn). A higher annealing temperature will reduce the solute segregation at dislocations in two ways. First, the magnitudes of the elastic constants will decrease and so does the effective interaction energy. The lowered interaction energy will lead to the less segregation. Second, a higher temperature will provide the solute atoms and matrix with more thermal energy which drives the solute atoms away from the dislocations. Thus to get the yield point phenomenon in a crystal containing solute atoms, the annealing temperature should be low enough to ensure the segregation, but high enough to allow the diffusion of the solute atoms.

V. CONCLUSIONS

The anisotropic linear elasticity was applied to the solute-dislocation interaction in Zn crystals and the following new conclusions were obtained:

1. The application of the anisotropic elasticity can reveal important details of interaction energies and force-displacement relations which have not been found by the isotropic approach.
2. For a Cd solute atom, the lowest gradient of the anistropic interaction energy due to the "size" effect lies in the direction predicted by the isotropic approach, while for a Ag solute atom, this gradient is highly deviated from such direction.
3. If the conventional lower limit of one Burger's vector of the linear elasticity is adopted, then the anisotropic elasticity gives 0.37 eV and 0.39 eV for Ag and Cd respectively as the binding energies of a solute atom to an edge dislocation due to the "size" effect in Zn, while the isotropic method gives 0.16 eV and 0.22 eV respectively.
4. Different sources of interactions, when combined, can influence additively the total interaction energy, but affect the total force-displacement relation for rigid glide of a straight dislocation in a more complicated way.
5. The core correction and the vibrational entropy effect can reduce the solute concentration within the core by orders of magnitude.

PART 2. EQUILIBRIUM CONFIGURATION OF DISLOCATION IN THE STRAIN FIELD OF SUBSTITUTIONAL SOLUTE ATOMS

I. INTRODUCTION

Current theories[41-45] on the "solution hardening" employ at least one of the following three assumptions: i) Solute atoms are point obstacles; ii) Dislocation lines are flexible string with a constant line tension; and iii) Dislocation lines bow out in circular arcs between the point obstacles when subjected to an external shear stress. All the computer simulations[16-18] of dislocation motions through the random distribution of solute atoms, and subsequent statistical analyses[19-22] of thermally activated motion of the dislocations through such distributions, have been based on essentially all three assumptions. In the framework of linear elasticity, however, a solute atom acts as an internal strain center with a certain influence range, and induces positive and negative shear stress fields on the dislocation glide plane of the surrounding matrix, as shown earlier. Thus the dislocation shape will be affected by the shear stress fields of the solute atom itself.

Our purpose in this Part 2 is to examine the relevance of those three assumptions, especially the first and third ones. The examination will be done by computing the equilibrium configurations of dislocation lines which are determined by a balance between the shear stress fields of solute atoms, dislocation line tension and externally applied shear stress on the glide plane. Our detailed analysis will be proceeded based on the following assumptions:

(a) The dislocation-solute interaction is governed by the isotropic linear elasticity.

(b) The dislocation-solute interaction is due to the "size" effect only.

(c) There are no solute-solute interactions.

(d) Solute atoms only in the first nearest atomic layers parallel to the glide plane are considered.

(e) Solute atoms are distributed in square arrays over the glide plane.

(f) Dislocation lines are flexible and extensible strings with a constant line tension.

We take account of the fact that exactly one half of the solute atoms are attractive strain centers and the other half are repulsive ones under the assumption (b). We will show that the assumption (f) of the constant line tension can be removed from the present investigation.

Using the same set of assumptions, Stefansky and Dorn[27] have shown that for extremely low concentrations, the flow stress in the square arrays of the solute atoms increases asymptotically with the square root of the concentration, as prediced by existing theories.[41,42] They have shown also that as the concentration increases, the increasing rate of the flow stress slows down, and eventually the flow stress itself begins to decrease. Nevertheless, it will be shown that even for relatively high concentrations, the approximations of point obstacles and circular bowing of dislocation lines are justifiable to the remarkable accuracy. It will be also shown that the strengths of attractive and repulsive solute atoms are not identical in conflict with some earlier approaches.

II. SUMMARY OF THE EXISTING THEORIES

In this section, three existing theories will be briefly reviewed, because they are considered to contain some important or disputable concepts which can be clarified by the analysis in the sections following this summary.

A. Theory of Mott and Friedel[46]

This theory is based on the idea that dislocations in an alloy are not rigid straight lines as originally conceived by Mott and Nabarro. Instead they tend to be wavy in order to minimize their total energy in the stress fields of the solute atoms.

In a random solid solution, one half of the solute atoms adjacent to the glide plane will be attractive, and according to Friedel, the dislocation line will zigzag from one attractive solute to another. Then the flow stress is determined by a balance between the dislocations tendency to minimize its length and its attraction to solute atoms. Cutting of the solute atoms by the dislocation line is the same whether they are attractive or repulsive, but only the attractive solute atoms are assumed to determine the zigzag in this theory.

The theory is formulated in terms of the triangular array of attractive solute atoms as shown in Fig. 10. A dislocation prefers the zigzag configuration ABC to the straight line configuration X-X' as in passing from the latter to the former it gains more in interaction energy than it loses in line energy. The interaction energy gained per unit length along X-X' is

$$E_1 \simeq U_I/x \simeq \frac{U_I C_o}{b^2} \; y$$

where U_I is the total interaction energy and C_o is the solute concentration on the glide plane. The solute atoms are regarded as point obstacles and U_I is equal to the maximum absolute value of Eq. (4). The increase in the total line energy is

$$E_2 \simeq \frac{\Gamma}{x} \left[\sqrt{x^2+y^2} - x\right]$$

where $\Gamma = Gb^2/2$ is the dislocation line energy per unit length.

By minimizing $E_1 - E_2$ with respect to y, Friedel obtains the triangular distribution that gives the minimum barrier to the moving dislocation. Then the flow stress σ at 0°K, i.e. the stress required to move the dislocation from a stable configuration ABC to an equivalent configuration is given approximately by,

$$\sigma \simeq \frac{1}{2} G \varepsilon C_o$$

B. Friedel's Forest Model[41,46]

Even though Friedel has set this model to explain the dislocation cutting of unattractive forest dislocations, some authors apply this model to the solution hardening, because the assumptions are based on the point-obstacle concept. In the following review, we replace the term "unattractive forest dislocations" by "solute atoms".

Substitutional solute atoms are randomly distributed on the glide plane as illustrated in Fig. 11. A dislocation initially held by A, B, C overcomes the solute atom B by an external stress, σ_F, and then bows out under the same force to meet a new solute atom D after moving a distance y. The radius of curvature, R, for the arc ADC is determined

by

$$R = \Gamma/\sigma_F b \tag{17}$$

where Γ is the dislocation line energy. Then it can be easily shown that x is given by

$$2yR \simeq x^2 \tag{18}$$

where x is the distance between two adjacent solute atoms along the dislocation line. If the shaded area S is on the average equal to the area ℓ_S^2 per solute atom, where ℓ_S is the average spacing between solute atoms on the glide plane, then

$$S = \ell_S^2 = b^2/C_o \simeq xy \tag{19}$$

From Eqs. (15) to (17), we have

$$x = (Gb\ell_S^2/\sigma_F)^{1/3} \tag{20}$$

if we put $\Gamma = Gb^2/2$. Assuming the external work $\sigma_F b\, x\, d$, where d is the distance moved by the dislocation to cut the solute atom B, is equal to the total interaction energy U_I of the solute atom B with the dislocation, and putting $d \simeq b$, from Eq. (20), we have

$$\sigma_F = (U_I^3/Gb^9)^{1/2}\ C_o^{1/2} \tag{21}$$

If the maximum absolute value of interaction energy due to the "size" effect is taken on for U_I from Eq. (4), σ_F becomes

$$\sigma_F = (\tfrac{1}{8}\, G^3 b^9 \varepsilon^3/Gb^9)^{1/2}\ C_o^{1/2} = \frac{1}{2\sqrt{2}}\, G\varepsilon^{3/2}\ C_o^{1/2} = \frac{1}{2\sqrt{2}}\, G\varepsilon^{3/2}/\ell_S \tag{22}$$

C. Fleischer's Theory[42]

In this theory also, a random distribution of solute atoms is assumed and the flow stress at 0°K is determined by an averaging process. A dislocation cutting a solute atom B will bend by an angle θ at an adjacent solute atom A as shown in Fig. 12. Fleischer assumes that the area swept by the dislocation is equal to the average area ℓ_S^2 per solute atom. Thus

$$x^2\theta/2 = \ell_S^2 = b^2/C_o \tag{23}$$

When the force F_m due to the applied stress, σ_L, which is given by

$$F_m = \sigma_L x b \tag{24}$$

is balanced with the force due to the dislocation line energy such that

$$F_m = 2\Gamma \sin(\theta/2) \tag{25}$$

then the dislocation segment CAD can overcome the solute atom A without thermal activation. Then from Eqs. (23) to (25) and with $\Gamma = Gb^2/2$, we have

$$x = (Gb\ell_S^2/\sigma_L)^{1/3} \tag{26}$$

This is exactly the same as Eq. (20) by Friedel. Then by substituting Eq. (26) into Eq. (24), the flow stress at 0°K is given by

$$\sigma_L = (F_m^3/Gb^b)^{1/2}\ C_o^{1/2} \tag{27}$$

If we note $F_m = U_I/d$, and then use the "size" effect for U_I, σ_L will be exactly the same as σ_F in Eq. (21).

The constant line tension, the circular bowing of dislocation between obstacles [Eq. (17)], and the line energy force on the obstacles [Eq. (25)] in the last two theories constitute the concept of the "point-obstacle", on which the computer simulations[16-18] and statistical analyses[20-22] are based. We will return to this point-obstacle approximation later. One interesting feature of the last two models is that if a new stress σ^* is defined such that $\sigma^* = \sigma \cdot \ell_S$, then σ^* is independent of ℓ_S or C_o, as can be seen from Eq. (22). We will show that our numerically computed flow stresses approaches asymptotically a constant value as ℓ_S increases.

III. FORMULATION

In this section, we will adopt the formulation by Stefansky and Dorn[27] in a square array of substitational solute atoms on the glide plane. The formulation will lead to a differential equation which determines the equilibrium configurations of a dislocation introduced into the square array at various external shear stress levels. Actually the solute atoms will be distributed rather at random over the glide plane. However, the equilibrium shapes of dislocation in the shear stress fields of solute atoms can be exactly solved only in simple regular arrays because of the simplicity in formulation and computation. Such an analysis would be almost impossible in random arrays of solute atoms unless some arbitrary assumptions are used.

If the dislocation-solute atom interaction is attributed to the "size" effect, a gliding dislocation line will, on the average, pass equal numbers of attractive and repulsive solute atoms. Thus, a square array shown in Fig. 13 will be the simplest regular array. In Fig. 13, we set the origin of the cartesian coordinates at one of the repulsive solute atoms and label each solute atom with two indices, m and n. Let the glide plane be the (111) plane in FCC crystals and ℓ_s be the spacing between solute atoms. Let our substitutional solute atoms be oversized, and then the size misfit parameter ε will be positive. If $\varepsilon>0$, the solute atoms in the atomic planes above the glide plane will be repulsive obstacles and the solute atoms in the lower atomic planes will be attractive ones, as is clear from Eq. (1). Then for repulsive solute atoms, h in Eq. (1) is $b/\sqrt{6}$ while for the

attributive ones h is $-b/\sqrt{6}$. Therefore, if our glide plane is infinite in extent, the shear stress (with the core correction introduced earlier) at a point (x,y,o) on the glide plane due to the entire solute atoms on the first atomic planes above and below the glide plane will be given by

$$\tau_{yz} = \frac{6G\varepsilon r_o^3}{\sqrt{6}} \sum_{m,n=-\infty}^{\infty} (-1)^{m+n} \frac{(y-n\ell_s)\left\{1-e^{-\left(\frac{3}{b^2}\right)[(x-m\ell_s)^2+(y-n\ell_s)^2+b^2/6]}\right\}}{[(x-m\ell_s)^2+(y-n\ell_s)^2+b^2/6]^{5/2}} \tag{28}$$

Now we introduce an edge dislocation into the square array of solute atoms such that the Burgers vector is parallel to the y-axis and the dislocation line is parallel to the x-axis, and then we let the dislocation relax to its minimum energy configuration in the stress fields, τ_{yz}, of the solute atoms. Because of the nature of the alternating distribution of solute atoms, the equilibrium configuration of the dislocation line $y = y(x)$ will be a periodic function of x with a period of $2\ell_s$. The total energy of a dislocation line[47] will then be

$$U = U_o + \int_{-\ell_s}^{\ell_s} \left\{\Gamma\left[\sqrt{1+(dy/dx)^2} - 1\right] - \int_0^y \tau_{yz} b dy - \tau b y\right\} dx \tag{29}$$

where U_o is the energy of a straight dislocation segment of length $2\ell_s$ lying parallel to the x-axis at $y = 0$, Γ is the line tension of the dislocation per unit length, and τ is a resolved shear stress of the externally applied stress on the glide plane.

The equilibrium shape, $y = y(x)$, of the dislocation can be obtained by applying the calculus of variation to minimize U. Then U must satisfy the Euler equation,

$$\frac{d}{dx}\left(\frac{\partial U}{\partial p}\right) - \frac{\partial U}{\partial y} = 0 \quad ,$$

where $p=dy/dx$. From this we obtain the differential equation for the equilibrium configuration

$$\frac{d^2y/dx^2}{\{1+(dy/dx)^2\}^{3/2}} = -\frac{b}{\Gamma}(\tau + \tau_{yz}) \ . \tag{30a}$$

The left-hand side of Eq. (30a) is equal to the curvature of the dislocation line. Thus if τ_{yz} is not considered, then Eq. (30a) will be equivalent to Eq. (17).

For computation it is more convenient to introduce dimensionless variables by letting $X=x/b$, $Y=y/b$. For the edge orientation, the line tension Γ is given by $3Gb^2/4$.[48] Thus Eq. (30a) may be transformed to

$$\frac{d^2Y/dX^2}{[1+(dY/dx)^2]^{3/2}} = -\frac{4}{3}(\tau/G + \tau_{yz}/G) \tag{30b}$$

where, by letting $r_o=b/2$ and $L_s=\ell_s/b$ in Eq.(28), τ_{yz}/G is given by

$$\tau_{yz}/G = \frac{3\varepsilon}{4\sqrt{6}} \sum_{m,n} (-1)^{m+n} \frac{(Y-nL_s)(1-e^{-3R_{mn}^2})}{R_{mn}^5} \tag{31}$$

with

$$R_{mn} \equiv [(X-mL_s)^2 + (Y-nL_s)^2 + 1/6]^{1/2} \tag{32}$$

Equation (30b) is a second order non-homogeneous differential equation which can be solved numerically with two independent boundary conditions. Since our solutions should be periodic and hence symmetric about the y-direction, we can conclude that $dY/dX = 0$ at each solute atom, and thus we have the necessary boundary conditions.

IV. COMPUTATION AND RESULTS

A. Computation Algorithm

Equation (30b) contains three parameters: τ/G, L_s and ε, which can be fixed to some constant values. The computations were performed numerically. A computer code was programmed such that a series of trial values Y_o of Y at X = 0 were picked up until the desired curve Y = Y(X) having zero slop at $X = L_s$ was obtained. For a trial value of Y_o, dY/dX at X = 0 was always put equal to zero, and the construction of the solution curve Y = Y(X) was performed by using a fifth order Runge-Kutta method.[49] This method involves essentially step-by-step solution of Eq. (30b) over the interval $0 \leqslant X \leqslant L_s$, and it requires that the initial conditions be known at the starting point X = 0. In order to obtain the flow stress at 0°K, the parameter τ/G was increased to a series of new values, holding L_s and ε constant. As τ/G approaches the flow stress, the position and shape of the dislocation line change gradually. If τ/G exceeds the flow stress, dY/dX is nonzero at $X = L_s$ for all possible values of Y_o. Thus in this way the flow stress can be approximated as closely as desired. In the present work, the flow stress was computed to an accuracy of about ± 0.1%.

B. Results for Alternating Arrays

The equilibrium configurations of dislocation line and the flow stress required for a dislocation to sweep through the solute atoms in the square array were computed. The size misfit parameter $\varepsilon = 0.06$ was used for all the computations. A sequence of the equilibrium configurations of dislocation line with τ increasing from zero to a stress level close to the flow stress in an alternating array (with $\ell_s = 20b$) of repulsive (R)

and attractive (A) solute atoms is shown in Fig. 14. Solute atoms are represented in dotted circles only to show their positions along the x-axis.

When $\tau=0$, the dislocation line zigzags in a triangular shape and rounds off slightly within a range of one Burger's vector around each solute atom. When τ increases, then the dislocation line gradually bows out between the solute atoms. Fig. 15 shows the equilibrium configurations of dislocation line (in solid lines) at the flow stress levels for a series of ℓ_s's. The scales along the x-axis were distorted to emphasize the gradual change in the shape of the dislocation line. As the solute atom spacing, ℓ_s, increases, the dislocation line bows out deeper and deeper between solute atoms. These equilibrium configurations in Fig. 15 are somewhat different from the configuration, shown schematically in Fig. 16 which Stafansky and Dorn[27] describe as a representative case of their computed equilibrium configurations. They seem to have computed the equilibrium configurations for $\ell_s \lesssim 15b$, using a less accurate numerical method. Their description of the configurations is consistent with the present results when $\ell_s \lesssim 15b$, but seems to be incomplete when $\ell_s \gtrsim 15b$.

The distances on the y-axis between the repulsive solute atoms and the dislocation lines are 0.25b to 0.30b. This indicates that the flow stress (or the instability of the equilibrium configuration) is determined by the dislocation configuration around the repulsive solute atoms rather than the configuration around the attractive ones in the present alternating arrays. Actually, the peak of the shear stress field of our substitutional solute atom is 0.2525b away from the

physical center of the solute atom itself. We will return to this point later.

In Fig. 17, the flow stresses, τ_Y/G, was plotted in a solid line against b/ℓ_s. This quantity, b/ℓ_s, is equivalent to the average concentration, C_o, of solute atoms, as is clear from Eq. (23). As ℓ_s decreases, the flow stress, τ_Y, increases gradually, but the increasing rate gradually slows down, and as ℓ_s becomes smaller than about 10b, then τ_Y passes a peak and decreases thereafter. As is clear from Fig. 15, a dislocation line tends to be more straight as ℓ_s decreases. A straight dislocation will be equally pushed and pulled by the solute atoms of opposite signs. Thus the strengthening effect due to higher concentrations of solute atoms will be eventually diminished as pointed out by Mott and Nabarro[7-9] and again Stefansky and Dorn.[27]

C. Dislocation Configurations and Flow Stresses in Unmixed Arrays

In addition to the flow stresses for the alternating arrays, we also computed the flow stresses for square arrays of purely repuslive solute atoms and purely attractive solute atoms. In the actual computations, $(-1)^{m+n}$ in Eq. (32b) was replaced by (-1) for repulsive and by (+1) for attractive square arrays, respectively. The computed flow stresses for square arrays of repulsive solute atoms with the size misfit $\varepsilon=0.06$ were plotted in a dashed line in Fig. 17. As predicted by Eq. (22), the flow stress increases linearly with $1/\ell_s$. It is noticed that the flow stress for alternating arrays approaches asymptotically the flow stress for repuslive arrays as the solute atom spacing, ℓ_s, increases. In Fig. 18 we plotted τ_Y vs ℓ_s in a slightly

different way. By defining a new dimensionless flow stress τ_Y^* such that $\tau_Y^*=\tau_Y b\ell_s/2\Gamma$, which is used in some statistical analysis[21] of random arrays of point obstacles, we can compare different arrays on a basis of a fixed numerical constant. As is shown in Fig. 18, the flow stresses, τ_Y^*, for the repulsive and attractive arrays are independent of ℓ_s while τ_Y^* for the alternating arrays increases at first and then asymptotically approaches τ_Y^* for the repulsive arrays.

The flow stresses, τ_Y^*, for the attractive arrays turned out to be slightly higher than those for the repulsive arrays, as is shown in Fig. 18. This is in conflict with the common practices[46] that the flow stresses for both arrays is taken to be the same. Figures 19a and 19b show only portions of dislocation lines (plotted in solid lines) for two stress levels in the immediate neighborhood of a solute atom in the repulsive and attractive arrays with ℓ_s=10b, respectively. The equilibrium configurations in the two types of arrays are very similar except the relative positions of dislocation lines with respect to the center of the solute atom. A closer examination on the equilibrium configurations shows that the curvatures of the dislocation lines for attractive arrays are greater than those for repulsive ones at the same external stress levels. This means that dislocation lines in attractive arrays tend to be more undulated than those in repulsive arrays. To shed a light on this difference, we computed the shear stress field of each type of solute atoms using Eq. (1) with the core correction of Stafansky and Dorn and then plotted (in dashed lines) the positive (or repuslive) side of the stress field contours in

Figs. 19a and 19b. Comparing two figures of Figs. 19a and 19b, we can find that dislocation lines in an attractive array should climb up a steeper slope of the back shear stress hill of solute atom than such a slope in a repulsive array. We will show how a steeper slope can lead to a greater curvature and hence a greater flow stress level in the discussion section.

V. POINT OBSTACLE APPROXIMATION

Despite the frequent use of the point obstacle approach such as in theoretical problems (e.g., Refs. 19-22, 41, 42 and 51) in which the dislocation-obstacle interaction is involved, the approximations used in the approach have not been studied in detail. By following our previous work,[50] a formal basis for the point obstacle approximation to the interaction between a dislocation and a circularly symmetric obstacle will be presented in this section. The result will be applied to our substitutional solute atom interaction with dislocations.

Consider a physical obstacle whose interaction with a gliding dislocation is circularly symmetric in the glide plane and has an effective range (d') which is small compared to the average separation of obstacles (ℓ_s). Assume the dislocation is acted on by a resolved shear stress τ and consider that portion of the dislocation which is pressed against a particular obstacle. The local equilibrium configuration of the dislocation line will appear roughly as shown in Fig. 20. The total energy of this configuration may be written

$$E = \int_L \Gamma dl + \tau b A_L + W \tag{33}$$

where Γ is the line energy of the dislocation and the integral is taken over the portion (L) of the dislocation line included in the figure; A_L is the area behind L and $\tau b A_L$ measures the potential energy of L under applied stress τ; and W is the total energy of the interaction of L with the obstacle. In the square arrays E is equivalent to Eq. (29).

Using a two dimensional form of Gibbs[52] construction (illustrated in Fig. 20) the obstacle may be formally reduced to a point and the

energy W localized. Given that d' is small we enclosed the obstacle in an imaginary circle (D) of small radius d appreciably greater than d'. Only the portion of L within D is perturbed by the obstacle. We then extrapolate the arms of L into D until they meet at a point (x). Let the extrapolated lines represent the dislocation within D and let the point of intersection represent the obstacle. The total energy of this hypothetical configuration (L') is

$$E' = \int_{L'} \Gamma dl' + \tau b A_{L'} + W' \quad , \tag{34}$$

which is identical to E if

$$W' = W + \int_{D} \left\{ \Gamma(dl - dl') + \tau b \; (dA_L - dA_{L'}) \right\} \tag{35}$$

If the dislocation is in mechanical equilibrium, there must be no possible variation of L (or, equivalently, of L') which causes the energy to decrease. As may be easily seen by considering variations which leave the position of the point (x) in L' unchanged, it is necessary for equilibrium that W' have its minimum value, W'(x), consistent with the position (x) and the configuration of L outside of D, and L' be symmetric about a line (l) through x and the physical center of the obstacle. If L' satisfies these conditions and if it is in equilibrium with respect to all variations which carry x along l and constrain W' to W'(x), then it is in equilibrium with respect to any variation whatever. Hence from Eq. (34), L' is in mechanical equilibrium only if

$$\delta E' = \int_{L} (\Gamma/R - \tau b) \; \delta x_n dl' + \; dW'/dx_l - 2\Gamma \cos\psi/2 \; \delta x_l \geq 0 \tag{36}$$

In this equation, R is the radius or curvature of the element dl' of L and δx_n is the normal displacement of this element. The angle ψ is the angle formed by L' at the intersection point x and the term involving ψ accounts for the net change in line length L' due to the displacement of δx_l of x along l.

Since the variations δx_n and δx_l are independent and may have either sign, the inequality[36] yields two necessary conditions for equilibrium:

$$(1) \quad \tau b = \Gamma/R \tag{37}$$

everywhere on L' and

$$(2) \quad F = dW'/dx_l = 2\Gamma\cos\psi/2 \tag{38}$$

at the intersection point x. These conditions are the central equations of the point obstacle approximation as described earlier. Actually, Eq. (37) is equivalent to Eq. (17) and Eq. (38) is also equivalent to Eq. (25), because $\psi = \pi-\theta$

Equation (38) may be used to generate a mechanical force-displacement relation for the dislocation-obstacle interaction in the point obstacle representation. Thus, function $[F(x_l)]$ is obtained by displacing or deforming the unperturbed segments of the dislocation (for example, by increasing the applied stress) so that the dislocation passes through the obstacle while maintaining an equilibrium configuration. The resulting function $[F(x_l)]$ will be insensitive to the precise configuration of obstacles when $R \gg d$, and will be insensitive to the obstacles separation, ℓ_s, when $\ell_s > d$. When these two conditions are satisfied the force-displacement relationship is a fixed property of the representative point

obstacle. In the limit $\ell_s >> d$ the finite displacement of the dislocation in sweeping through the obstacle may be ignored. The obstacle may then be treated as a mathematical point which influences the dislocation only when in physical contact with it.

We applied this method of point obstacle representation to our substitutional solute atoms in repulsive and attractive square arrays. A sequence of computed equilibrium configurations of dislocation in a repulsive square array with $\varepsilon=0.06$ and $\ell_s=10b$ is illustrated in solid lines in Fig. 21. The scale of the figure has been distorted to allow clear distinction between the different configurations. The three lower dislocation lines are stable equilibrium configurations assumed with increasing applied stress; the two upper dislocation lines are unstable equilibrium configurations for a dislocation which has passed the peak of the positive side of the back shear stress field of a solute atom in the array. We have also shown in dotted lines the point obstacle representation of each configuration, by drawing an osculating circle to each equilibrium configuration. The discrepancy between the true and approximated dislocation configurations is significant only in the vicinity of the obstacle ($\lesssim 1b$).

The point obstacle force-displacement relation computed by applying Eq. (38) to this case is illustrated in a solid line in Fig. 22a. The same relation computed for an attractive solute atom with the same size misfit ($\varepsilon=0.06$) in a square array with the same period $\ell_s=10b$ is also illustrated in a solid line in Fig. 22b. In a previous work (e.g., Ref. 51) the force displacement relation for rigid motion of a straight dislocation through the solute atoms was used as an approximation to the dislocation-

point obstacle interaction. The force-displacement relation for rigid motion was computed under the assumptions of the above-mentioned two cases: repulsive and attractive square array (with ℓ_s=10b) of solute atoms (with ε=0.06) from Eq. (5) and is compared to our force-displacement relations for the flexible dislocation-point obstacle interaction in dotted lines in Figs. 22a and 22b. The agreement between the two curves in each figure is good. Use of our point-obstacle representation results in a slight increase in the maximum forces and small shifts in the position of the maximum with respect to the physical center of the solute atom. Since the dotted lines in both figures should be exactly symmetric with respect to the force axis. We can compare the two solid lines through the dotted lines, we can find here once again that an attractive solute atom is a stronger obstacle than a repulsive solute atom.

Further computations indicated that the force-displacement relation is reasonably insensitive to the solute atom spacing $\ell_s \gtrsim 4b$ as can be anticipated from the upper two stress levels for the repulsive and attractive square arrays in Fig. 18.

VI. DISCUSSION

This section is divided into four subsections and appropriate discussions are given on the following five topics in order: i) relevance of the assumptions, ii) relative strengths of the repulsive and attractive arrays, iii) point-obstacle approximation, and iv) a new problem raised from the present study.

A. Relevance of Assumptions

The assumptions listed in the introduction section are made to simplify our analysis in the next sections. Thus the isotropic linear elasticity on which the current theories on the dislocations are based seems to be the most appropriate assumption. The anisotropic elasticity may be adopted, but undoubtedly it will make a very complicated analysis. In addition to the "size" effect, other sources of dislocation-solute interaction can be also considered in principle. However, expressions of the back shear stress on the glide plane, equivalent to Eq. (1) due to the "size" effect are not available yet in simple forms like Eq. (1) for these other sources.

The elastic solute-solute interaction can be neglected safely when the inter-solute atom spacing, ℓ_s, is larger than the effective range of about 3b. When ℓ_s is less than 3b, the back stress fields of solute atoms overlap each other as shown by Stefansky and Dorn,[27] and then the elastic solute-solute interaction must be accounted. The short range ordering of solute atoms will lead to clustering of solute atoms[5] in conflict with our model of regular arrays in dilute solid solutions. Stefansky and Dorn[27] pointed out that solute atoms on the

second nearest atomic layers parallel to the glide plane are 25% as strong as the solute atoms in the first nearest atomic planes. Thus by constructing an appropriate regular array these solute atoms on the second nearest atomic planes can be fully accounted.

The regular array approach is relevant and justified in the sense that it allows the analysis of the equilibrium configuration of dislocation lines, which is practically impossible with the random array approach as mentioned earlier. The assumption of the constant line tension seems to be appropriate, because the deviations of the dislocation lines from the edge orientation were extremely small for the entire spectrum of ℓ_s's. The maximum slopes of the dislocation line with respect to the edge orientation were less than 3° for the size misfit parameter $\varepsilon = 0.06$. If ε is very large (i.e., strong solute atom) and hence the deviation cannot be neglected, by replacing the line tension term, Γ, by a suitable function of orientation and position, we can give a full correction for the deviation. Then we may have to solve a slightly different equation from Eq. (30-a). The elastic self interaction between segments of curved dislocation can be neglected from the same reason. Foreman[53] has shown that such second order effect is small, particularly in the case of weak obstacles.

B. Strengths of Repulsive and Attractive Arrays

Referring to Figs. 19(a) and (b), we will show here qualitatively why the steeper slope of the back stress field requires a higher flow stress in an attractive array than the less steep slope does in a repulsive array.

If the left-hand side of Eq. (30-a) is replaced by a new parameter K representing the curvature of dislocation line, and (-) sign on the right-hand side is dropped, then Eq. (30-a) is transformed to

$$K = b/\Gamma\ (\tau + \tau_{yz}) \tag{30-c}$$

Then the variation of the curvature in the y-direction will be determined by the slope of the shear stress field, τ_{yz}, along the y-direction as follows:

$$\partial K/\partial y = b/\Gamma \cdot \partial\tau_{yz}/\partial y \tag{39}$$

Thus under a constant external stress, τ, identical virtual displacements of dislocations by an infinitesimal distance along the y-direction will result in a greater increase in the curvature in an attractive array because of the steeper slope, $\partial\tau_{yz}/\partial y$ than in a repulsive array with the same distribution of solute atoms. Then small displacements of dislocation from the same initial level of τ_{yz} to the same final level of τ_{yz} will lead to a greater final curvature in the attractive array than in the repulsive array, if the initial curvature was the same in both arrays. To maintain a greater curvature, a greater external stress should be applied.

The difference in the flow stresses between the repulsive and attractive arrays is, however, not so significant as the difference in the slopes. This seems to be due to the following two facts, as is obvious from Figs. 19(a) and (b). First, the slope of the shear stress field decreases as a dislocation approaches the peak and ridge of the stress field. Second, the absolute magnitudes of the dislocation

curvatures are very small at all external shear stress levels. Thus as the dislocations continue to press on the attractive solute atoms, the curvature change becomes smaller, and the smaller curvature change influences the already very small curvature only insignificantly.

C. Point-Obstacle Approximation

In the point obstacle approximation of the dislocation-solute atom interaction, the equilibrium configuration of dislocation lines subjected to an external stress τ is represented by a circular arc between the equivalent point obstacles, the radius being determined by Eq. (37). As we have shown in a repulsive array in Fig. 21, this circle represents very accurately the true configuration of the dislocation line except in the immediate vicinity of the solute atoms. Even in this vicinity the maximum discrepancies between the two configurations are less than b/50. Even in the alternating arrays, the circular approximation seems to be excellent as is shown in dashed lines in Fig. 15, when the solute atom spacing, ℓ_s is greater than 10b.

The second feature of the point obstacle representation is that an obstacle will be cut if the angle ψ between two segments of dislocation held by the solute atom is less than a critical angle ψ_C as can be seen from Fig. 20. We measured this critical angle in the repulsive and attractive arrays from the equivalent circular configurations at the flow stress levels, and found that this critical angle does not change with the solute atom spacings. As anticipated, the critical angle ψ_C for the attractive arrays was slightly smaller than that for the repulsive arrays. Then we measured the angle ψ_C in the alternating

arrays from Fig. 15 and found that ψ_C varies widely at the attractive solute atoms but remains constant at the repulsive solute atoms even though the dimensionless flow stress τ_Y^* drops rapidly as ℓ_s decreases. The variation of critical angle ψ_C at the repulsive solute atom is illustrated in Fig. 23 in terms of $\cos(\psi_C/2)$ vs ℓ_s/b. Comparing Fig. 23 with Fig. 18, we can obtain an interesting conclusion that even in the alternating arrays of high solute concentration (~ 1%) the principle of critical angle works perfectly.

The fact that the two features of the point obstacle approximation are obeyed almost exactly in the repulsive or attractive arrays indicates that a dislocation motion through the distribution of discrete obstacles whose interaction with the dislocation is symmetric with respect to the glide plane can be predicted by the point obstacle approximation. By symmetric with respect to the glide plane means that the sign of the interaction energy is the same whether the obstacle is placed below or above the glide plane. In this sense, all the substitutional solute atoms with the size misfit $\varepsilon \neq 0$, are antisymmetric obstacles. The best example of the symmetric obstacles would be substitutional solute atoms with zero size misfit but with non-zero modulus misfit.

In Fig. 15, the dislocation line configuration in the alternating array with $\ell_s = 10b$ does not cross the x-axis, while the lines in the same arrays with higher ℓ_s cross it. However, in Fig. 24 we shift the repulsive solute atoms in the array with $\ell_s = 10b$ by 0.2525b upward along the y-direction and the attractive ones by the same distance downward such that the peaks of the positive sides of the back shear stress field of the repulsive and attractive solute atoms

are aligned on the x-axis. Then the flow stress τ_Y^*, increases from 0.02050 to 0.04603, by more than twice, and the dislocation configuration changes dramatically as shown in Fig. 24. Thus if we make a square array of solute atoms with their peaks of the positive sides of the back stress fields, not just with the geometrical centers of the solute atoms, the flow stress and equilibrium dislocation configuration will be precisely predicted by the rules of point obstacle approximation.

Thus the point obstacle approximation seems to be a really promising approach and all the computer simulations and the statistical analyses of dislocation motions through random arrays of discrete obstacles may be justified whether or not the obstacles are symmetric. However, this justification is not without a qualification. In the computer simulations[16-18] performed so far, a dislocation segment bowing out between two neighboring point obstacles does not recognize the existence of a third obstacle, no matter how close it might be until the segment literally touches the geometrical center of the third obstacle. In this connection, we investigated the perturbation of the equilibrium configuration of dislocation by a third obstacle and the result will be shown below.

D. Perturbation of Dislocation Configuration

The perturbation of the equilibrium configuration of dislocation lines by a third solute atom is likely more serious in the alternating arrays than in the repulsive or attractive arrays. Thus we introduced a third solute atom between two solute atoms in the alternating square array with $\ell_s = 20b$. Then we solved Eq. (30-b) demanding the zero-

slope boundary condition to be satisfied at the first and second solute atoms for various positions of the third solute atom.

The results are illustrated in Fig. 25 in dashed lines with respect to the unperturbed configuration in solid lines. The upper group represents the perturbed configurations by a repulsive third atom, while the lower group represents the perturbed shapes by an attractive one. The numerical values in the brackets preceded by the flow stresses represent the position of the third solute atom. The repulsive third atom distorts the configuration slightly when it is placed one Burgers vector away from the x-axis, but rather seriously when it is at one half of Burgers vector above the midpoint of the x-axis. The flow stress is increased substantially. The attractive third atom also perturbs the configuration slightly when it is one Burgers vector away from the x-axis, and the flow stress is decreased considerably, when the third one is above the x-axis. As the third solute atom deviates from the midpoint along the x-axis, the perturbation becomes more serious. When the attractive third is placed one half of Burgers vector below the x-axis, the distortion of dislocation is very serious and the flow stress is increased by more than twice. In any case of the configurations in Fig. 25, the perturbation effect of the third solute atom to the configuration of dislocation and flow stress is not ignorable at all, even though the third obstacle is not in physical contact with the dislocation. It is not clear yet whether the perturbations due to the attractive and repulsive third atoms in the alternating random arrays (arrays in which attractive and repulsive solute atoms are mixed at random) may cancel each other on the average

or not. Therefore, a compensation for the perturbation effect should be provided in a new, more realistic computer simulation or statistical analysis utilizing the point obstacle approximation, unless the perturbation effects are cancelled out by the solute atoms of opposite signs.

In this paper, all the computations were done by assuming the size misfit $\varepsilon = 0.06$. However, all the discussions and conclusions will not lose generality. Stefansky and Dorn[27] computed the flow stress variation with ε and found that the flow stress variation with ℓ_s maintains the same trend as appeared in Fig. 17.

VII. CONCLUSIONS

Dislocation interaction with substitutional solute atoms distributed in square arrays on the dislocation glide plane was studied and the following conclusions were obtained:

1. The force-displacement relations for cutting the stress fields of attractive and repulsive solute atoms are not identical in the point-obstacle representation of the solute atoms. A greater maximum force is required to cut attractive solute atoms as the slope of their effective opposing stress field is steeper than that of repulsive solute atoms.
2. The equilibrium configurations of dislocation lines can be approximated by the osculating circular arcs to a considerable accuracy and the cutting of solute atoms by dislocation lines can be exactly predicted by the critical-angle criterion of the point obstacle approach.
3. The perturbation of the equilibrium configuration of dislocation line by a third solute atom is not negligible in the implementation of the point obstacle approximation to the random array of solute atoms via computer simulations or statistical analyses, unless the perturbation effects are cancelled by the solute atoms of the opposite signs.

ACKNOWLEDGMENTS

Part 1 of this thesis is the outgrowth of research inaugurated by the late Professor John E. Dorn. Much of the work reported in Part 1 was done under his guidance.

I am deeply indebted to Professor J. W. Morris, Jr. for his constant interest and encouragement. Many valuable discussions with him were indispensable to complete this work. I also wish my appreciation to Professors J. Washburn and F. Hauser for reviewing the manuscript.

Thanks are due to Shirley Ashley and Jean Wolslegel for their swift and accurate typing, and to Gloria Pelatowski for preparing the figures.

I give the sincerest thanks to my wife Juyen, whose patience and support made it possible.

This work was done under the auspices of the U. S. Atomic Energy Commission.

APPENDIX

Estimation of Elastic Constants of FCC element in HCP Structure

In Fig. A1, the equivalence of atomic arrangement of the (111) plane of FCC structure and the (0001) plane of HCP structure is shown and the x-axis is drawn parallel to an edge dislocation line and the y-axis parallel to the Burgers vector of the dislocation line in each structure. The z-axis is perpendicular to the x- and y-axes and is coming out of the paper.

Due to the symmetry of stress and strain tensors, the tensor, $\underset{\sim}{c}$ of elastic constants, $c_{ijk\ell}$, is reduced to the matrix, $\{c\}$, of elastic constants of double indices, c_{ij}. The elastic constant matrix for hexagonal system, $\{c\}_h$, for the coordinate system shown in Fig. 2 is given by

$$\{c\}_h = \begin{bmatrix} c_{11} & c_{12} & c_{13} & 0 & 0 & 0 \\ c_{12} & c_{11} & c_{13} & 0 & 0 & 0 \\ c_{13} & c_{13} & c_{33} & 0 & 0 & 0 \\ 0 & 0 & 0 & c_{44} & 0 & 0 \\ 0 & 0 & 0 & 0 & c_{44} & 0 \\ 0 & 0 & 0 & 0 & 0 & c_{66} \end{bmatrix} \qquad \text{(A1)}$$

where $2c_{66} = c_{11} - c_{12}$ and indices 1, 2, and 3 correspond to the x-, y-, and z-axes, respectively.

The elastic-constant matrix, $\{c\}_c$, for the coordinate system x, y and z in any cubic system is given by

$$\{c\}_c = \begin{bmatrix} c_{11} & c_{12} & c_{12} & 0 & 0 & 0 \\ c_{12} & c_{11} & c_{12} & 0 & 0 & 0 \\ c_{12} & c_{12} & c_{11} & 0 & 0 & 0 \\ 0 & 0 & 0 & c_{44} & 0 & 0 \\ 0 & 0 & 0 & 0 & c_{44} & 0 \\ 0 & 0 & 0 & 0 & 0 & c_{44} \end{bmatrix} \qquad \text{(A2)}$$

This matrix, $\{c\}_c$, will transform to a new matrix, $\{c'\}_c$ when the coordinate system x, y and z transform to a new coordinate system x', y' and z' in Fig. A2 such that the x'-, y'- and z'-axes are parallel to the x-, y- and z-axes of Fig. A1, respectively. Thus $\{c'\}_c$ is given by[A1]

$$\{c'\}_c = \begin{bmatrix} c'_{11} & c'_{12} & c'_{13} & 0 & c'_{16} & 0 \\ c'_{12} & c'_{11} & c'_{13} & 0 & 0 & 0 \\ c'_{13} & c'_{13} & c'_{33} & 0 & -c'_{16} & 0 \\ 0 & 0 & 0 & c'_{44} & 0 & -c'_{16} \\ c'_{16} & 0 & -c'_{16} & 0 & c'_{44} & 0 \\ 0 & 0 & 0 & -c'_{16} & 0 & c'_{66} \end{bmatrix} \qquad \text{(A3)}$$

where $c_{11} = c_{11} + H/2$, $c'_{12} = c_{12} - H/6$, $c'_{13} = c_{12} - H/3$, $c'_{33} = c_{11} + 2H/3$, $c'_{44} = c_{44} - H/3$, $c'_{66} = c_{44} - H/6$, $c'_{16} = \sqrt{2}\, H/6$, and $H = 2c_{44} + c_{12} - c_{11}$. Thus by comparing Eqs. (A1) and (A3), we can choose elastic constants of FCC structures which are corresponding to those of HCP structures.

REFERENCES

1. A. H. Cottrell and B. A. Bilby, Proc. Phys. Soc. London, A62, 49 (1949).

2. H. Suzuki, Conference on Dislocation and Mechanical Properties of (Wiley, New York, 1957).

3. L. A. Jacobson, Ph. D. Thesis, University of California, Berkeley. UCRL Report #18310, 1968.

4. T. Suzuki, Proc. of Second Int'l Conference on Strength of Metals and Alloys, (ASM, Cleveland, 1970) p. 235.

5. N. F. Fiore and C. L. Bauer, Prog. Materials Sci. 13, 85 (1967).

6. W. G. Johnston and J. J. Gilman, J. Appl. Phys. 30, 129 (1959).

7. N. F. Mott, Imperfections in Nearly Perfect Crystal (John Wiley, New York, 1952) p. 173.

8. N. F. Mott and F. R. N. Nabarro, Report of a Conference on the Strength of Solids, (Physical Society of London, 1948), p. 1.

9. N. F. Mott and F. R. N. Nabarro, Proc. Phys. Soc. London, 52, 86 (1940).

10. S. K. Mitra and J. E. Dorn, Trans. AIME 224, 1062 (1962).

11. A. A. Hendrickson and M. E. Fine, ibid. 221, 967 (1961).

12. T. J. Koppenaal and M. E. Fine, ibid. 224, 347 (1962).

13. K. R. Evans and W. F. Flanagan, Phil. Mag. 16, 535 (1968).

14. T. Suzuki and T. Ishii, Physics of Strength and Plasticity, A. Argon, ed., (The MIT Press, Cambridge, 1969).

15. E. O. Hall, Yield Point Phenomena in Metals and Alloys, (Plenum Press, New York, 1970).

16. U. F. Kocks, Phil. Mag. 13, 541 (1966).

17. A. J. E. Foreman and M. J. Makin, Phil. Mag. 14, 911 (1966).

18. D. Klahn, D. Austin, A. K. Mukherjee and J. E. Dorn, Symposium on Statistical and Probabilistic Problems in Metallurgy, W. L. Nicholson, ed., Adv. Appl. Probability, Suppl, p. 112 (1972).

19. U. F. Kocks, Can. J. Phys. 45, 737 (1967).

20. A. S. Argon, Phil. Mag. 25, 1953 (1972).

21. J. E. Dorn, P. Guyot and T. Stefansky, Physics of Strength and Plasticity (The MIT Press, Cambridge, 1969) p. 133.

22. J. W. Morris, Jr. and D. Klahn, J. Appl. Phys., to be published.

23. J. D. Eshelby, Solid State Physics 3, 115 (1956).

24. W. T. Read, Dislocation in Crystals, (McGraw-Hill, New York, 1953).

25. J. Weertman and J. C. Weertman, Elementary Dislocation Theory (MacMillan, New York, 1964) p. 173.

26. A. H. Cottrell, Relation of Properties to Microstructure (ASM, Cleveland, 1954) p. 132.

27. T. Stefansky and J. E. Dorn, Trans. AIME, 245, 1869 (1969).

28. A. W. Cochardt, G. Schoeck and H. Wiedersich, Acta Met. 3, 533 (1955).

29. Y. T. Chou, J. Appl. Phys. 33, 2747 (1962).

30. R. L. Fleischer, Acta Met. 9, 996 (1961).

31. W. B. Pearson, Handbook of Lattice Spacings (Pergamon Press, London, 1958) p. 886.

32. H. B. Huntington, Solid State Physics 7, 213 (1958).

33. Y. A. Chang and L. Himmel, J. Appl. Phys. 37, 5767 (1966).

34. Constants at 473°K were extrapolated from the data by C. W. Garland and J. Silverman, Phys. Rev. 119, 1218 (1960).

35. J. M. Roberts and N. Brown, Acta Met. 10, 430 (1962).

36. R. M. J. Cotterill and M. Doyama, Phys. Rev. 145, 465 (1966).

37. F. Larché and J. W. Cahn, Acta Met. 21, 1051 (1973).

38. C. L. Bauer, J. Phys. Chem. Solids 27, 1133 (1966); Phil. Mag. 11, 827 (1965).

39. G. Alefeld, Phil. Mag. 11, 809 (1965).

40. D. O. Thompson, Proc. of Symp. Interactions between Dislocations and Point Defects, AERE-R 5994, p. 152, Harwell (1968).

41. J. Friedal, Electron Microscopy and Strength of Crystals, G. Thomas and J. Washburn, ed., (Interscience, New York, 1968) p. 605.

42. R. L. Fleischer, Acta Met. 11, 203 (1966).

43. B. R. Riddhagni and R. M. Asimow, J. Appl. Phys. 39, 4144 (1968).

44. O. Boser, J. Appl. Phys. 44, 1033 (1973).

45. R. Labusch, Acta Met. 20, 917 (1972).

46. J. Friedel, Dislocations (Addison-Wesley, 1964) Chapt. 15.

47. J. E. Dorn and S. Rajnak, Trans. AIME 224, 1052 (1962).

48. J. E. Dorn, Energetics of Dislocation Mechanisms, in N. R. C. Seminar on Energetics in Metallurgical Phenomena (Gordon and Breach, 1965).

49. R. L. Ketter and S. P. Prawel, Jr., Modern Methods of Engineering Computations, (McGraw-Hill, 1969) Chapt. 10. For computer subroutine, see the writeup of D2-CAL-RK5, Computer Center, University of California, Berkeley.

50. J. W. Morris, Jr. and C. K. Syn, J. Appl. Phys. (to be published).

51. L. J. Teutonico, A. V. Granato, and K. Lücke, J. Appl. Phys. 35, 220 (1964); A. V. Granato, K. Lücke, J. Sclipf and L. J. Teutonico, J. Appl. Phys. 35, 2372 (1964).

52. J. W. Gibbs, Scientific Papers, Vol. 1, p. 219, Dover, New York (1969).

53. A. J. R. Foreman, Phil. Mag. 15, 1011 (1967).

A1. J. P. Hirth and J. Lothe, Theory of Dislocations (McGraw-Hill, 1968) Chapt. 13.

FIGURE CAPTIONS

Fig. 1. Solute atom-dislocation geometry.

Fig. 2. Solute atom-dislocation geometry in an anisotropic hexagonal crystal. The solute atom is represented by principal strain components generated by itself.

Fig. 3. Anisotropic interaction energy contours for Ag (a) and Cd (b) solute atoms due to the "size" effect.

Fig. 4. Anisotropic interaction energy contours for Ag (a) and Cd (b) solute atoms due to the "modulus" effect.

Fig. 5. Anisotropic interaction energy contours for Ag (a) and Cd (b) solute atoms due to the "size plus modulus" effect.

Fig. 6. Force-displacement relations for rigid glide of an edge dislocation with respect to Ag solute atmosphere with and without corrections (see text).

Fig. 7. Force-displacement relations for rigid glide of an edge dislocation with respect to Cd solute atmosphere with and without corrections (see text).

Fig. 8. Variation of solute concentration C_{co} within the dislocation core with the average solute concentration C_o for Ag.

Fig. 9. Variation of solute concentration C_{co} within the dislocation core with the average solute concentration C_o for Cd.

Fig. 10. Friedel's triangular array of solute atoms.

Fig. 11. Dislocation held by point obstacles in a random array: Friedel's model.

Fig. 12. Dislocation bending around point obstacles in a random array: Fleischer's model.

Fig. 13. Alternating square array of repulsive (R) and attractive (A) solute atoms. The double indices are given to each solute atoms by the distances to the x- and y-axes in unit of intersolute spacing, ℓ_s.

Fig. 14. A series of equilibrium configuration of dislocation line at different external shear stress levels in the alternating square array of ℓ_s=20b.

Fig. 15. Variation of equilibrium configurations of dislocation line at the flow stress level in alternating arrays with ℓ_s=10b to 50b, increasing by 10b.

Fig. 16. A representative equilibrium configuration computed by Stefansky and Dorn.

Fig. 17. Variations of the flow stress τ_Y/G with b/ℓ_s.

Fig. 18. Variations of the flow stresses τ_Y^* with ℓ_s/b. For the definition of τ_Y^*, see the text.

Fig. 19. The equilibrium configurations of dislocation lines (in solid lines) in the positive side of the shear stress fields of solute atom (in dashed lines) in repulsive (a) and attractive (b) arrays. Only the portion in the vicinity of one solute atom in each array is illustrated.

Fig. 20. A geometric construction used to define the point properties of an obstacle having a circularly symmetric interaction with a dislocation.

Fig. 21. Sequence of equilibrium configurations of a dislocation (in solid lines) and their representations (in dotted lines) in a repulsive array of ℓ_s=10b. The physical center of the repulsive solute atom is placed at the origin of the coordinates.

Fig. 22. The force-displacement relations for the dislocation interaction with one repulsive (a) and one attractive (b) solute atoms. F is the force exerted by the dislocation on the obstacle at equilibrium as a function of distance from the physical center of the obstacle. The solid curves are computed from the point obstacle approximation by suing Eq. (38). The dotted comparison curves computed from Eq. (4) assume a rigid and straight dislocation.

Fig. 23. Variation of critical angles at the repulsive solute atoms in the alternating square arrays with ℓ_s/b.

Fig. 24. Equilibrium configuration of dislocation line at the flow stress level when the physical centers of repulsive and attractive solute atoms in an alternating array of ℓ_s=10b are shifted such that the peaks of the positive shear stress fields of the solute atoms are aligned. The physical centers are represented by crossed circles.

Fig. 25. Perturbed equilibrium configurations (in dashed lines) of dislocation lines by a third solute atom at various positions (represented by two numbers in the parenthesis) in an alternating square array of ℓ_s=20b are compared with the unperturbed configuration (in solid lines). Variation of the flow stress due to the perturbation is also shown by numbers preceding the parentheses.

Fig. A1. Equivalence of atomic structure of the (111) and (0001) planes in FCC and HCP structures respectively.

Fig. A2. The (111) plane in FCC structure and definition of the cartesian coordinates.

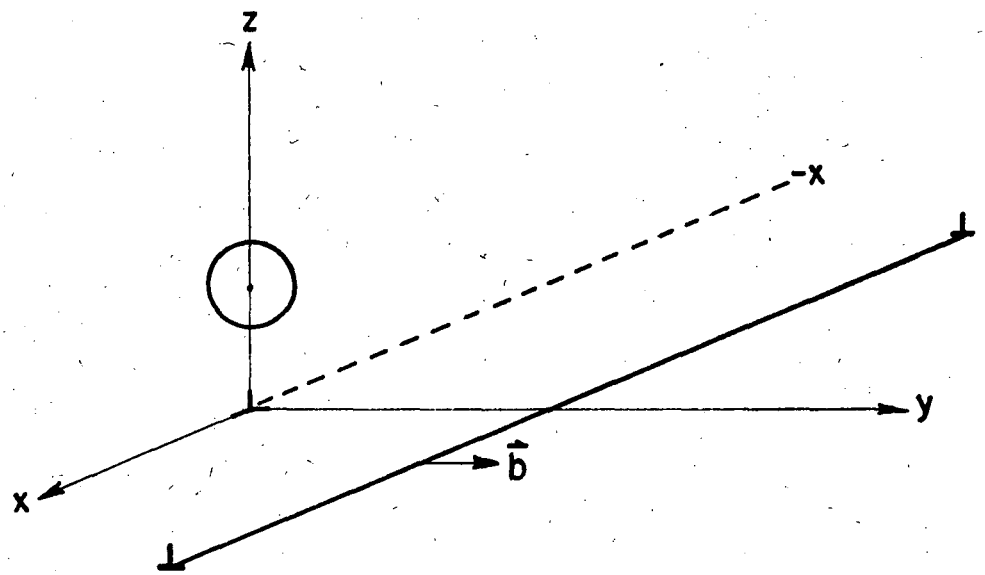

XBL 7310-5528

Fig. 1

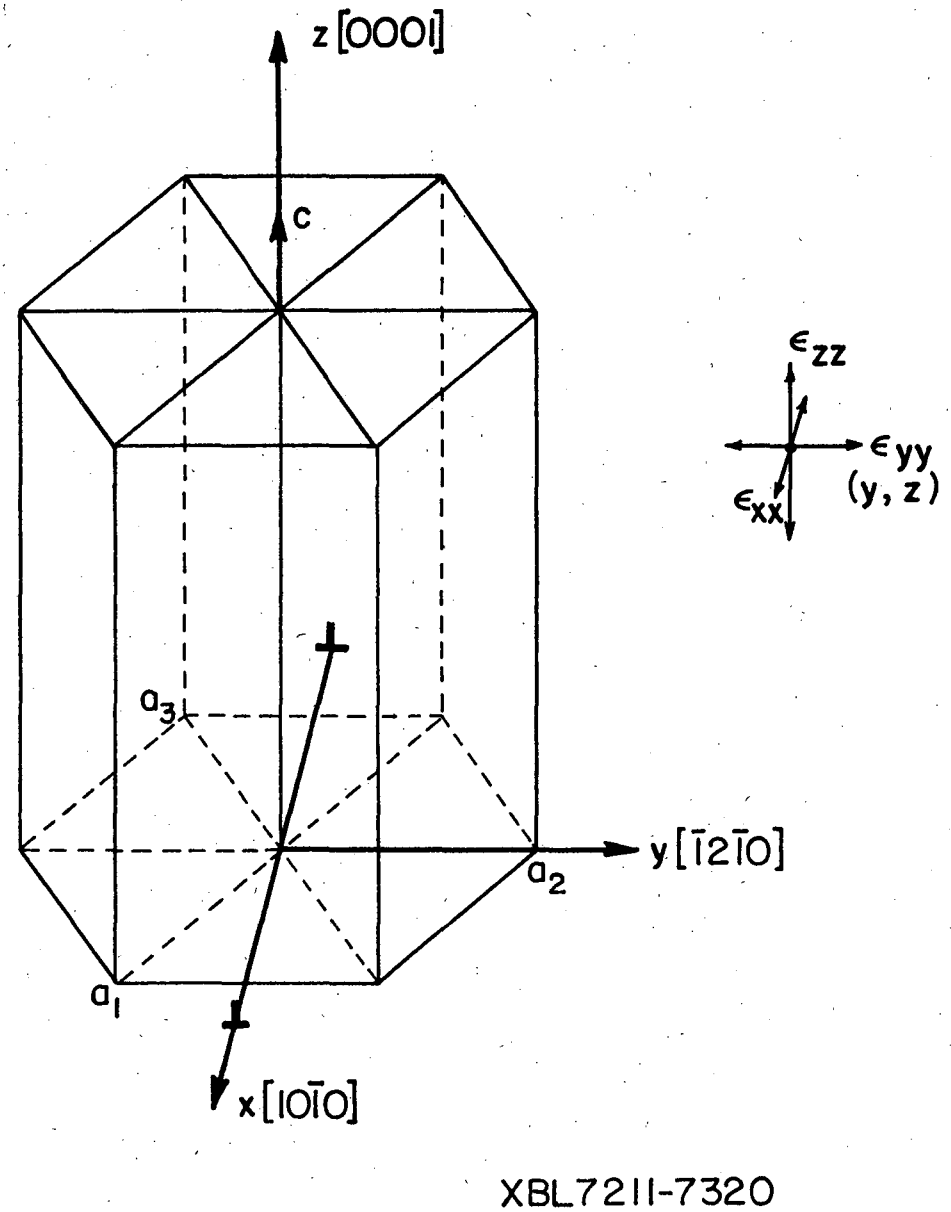
z [0001]
c
ϵ_{zz}
ϵ_{yy}
(y, z)
ϵ_{xx}
a_3
y [$\bar{1}2\bar{1}0$]
a_2
a_1
x [$10\bar{1}0$]
XBL7211-7320

Fig. 2

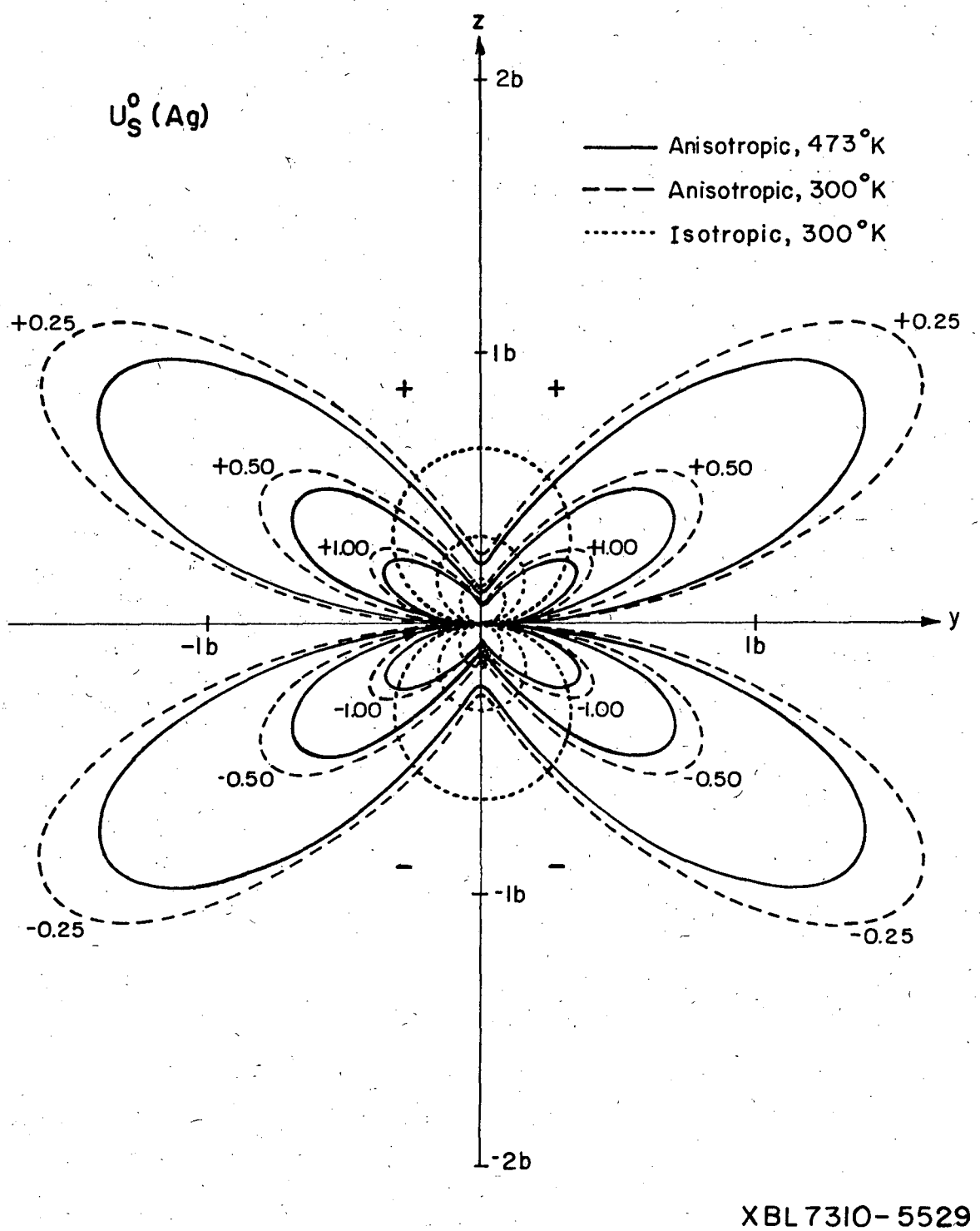
z
2b
U_S^0 (Ag)
Anisotropic, 473°K
Anisotropic, 300°K
Isotropic, 300°K
+0.25
+0.25
1b
+
+
+0.50
+0.50
+1.00
+1.00
y
-1b
1b
-1.00
-1.00
-0.50
-0.50
-
-
-1b
-0.25
-0.25
-2b
XBL 7310-5529

Fig. 3(a)

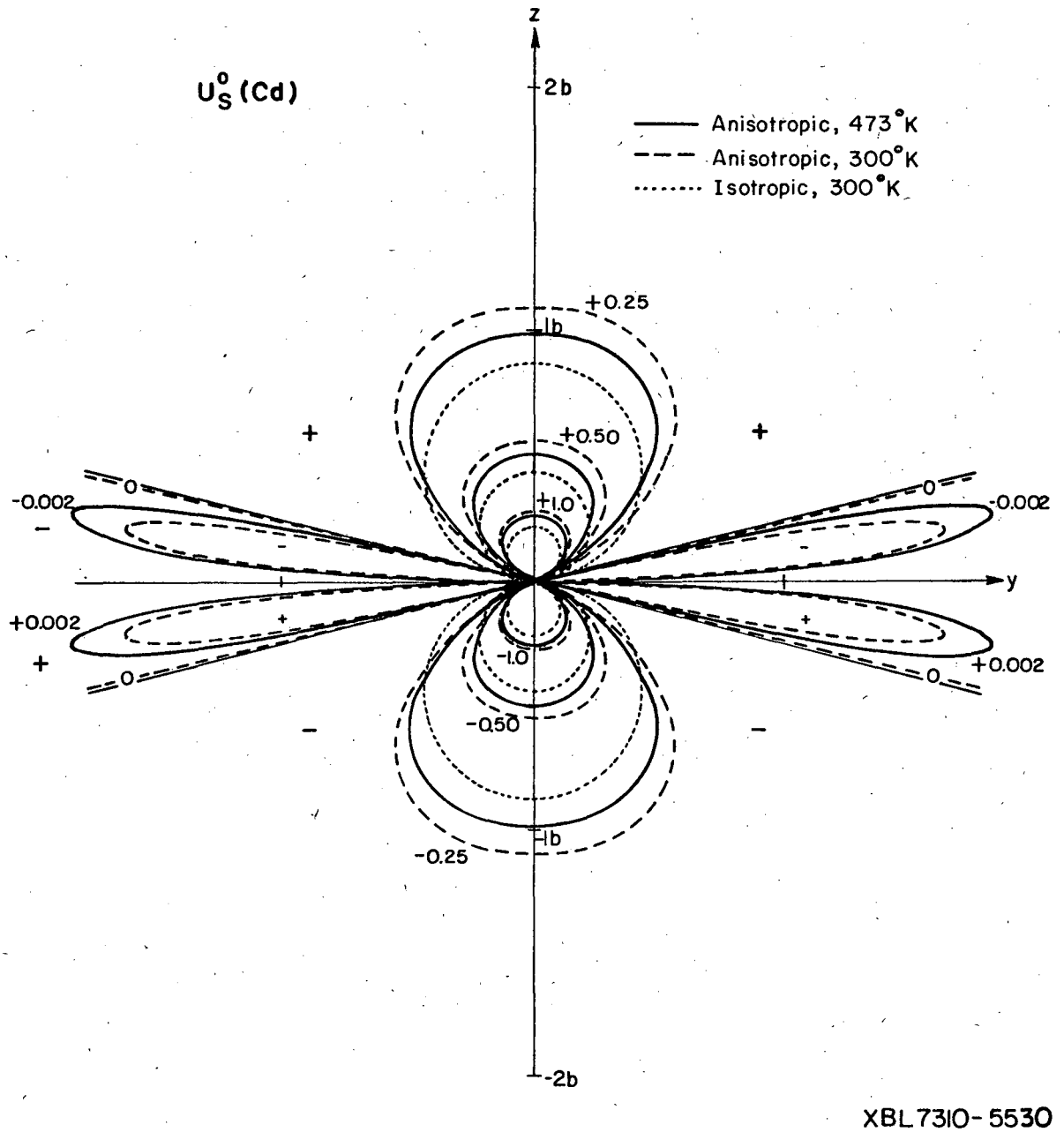
U_S^0 (Cd)
Anisotropic, 473°K
Anisotropic, 300°K
Isotropic, 300°K
z
y
2b
1b
-1b
-2b
+0.25
+0.50
+1.0
-1.0
-0.50
-0.25
0
-0.002
+0.002
+
-
XBL7310-5530

Fig. 3(b)

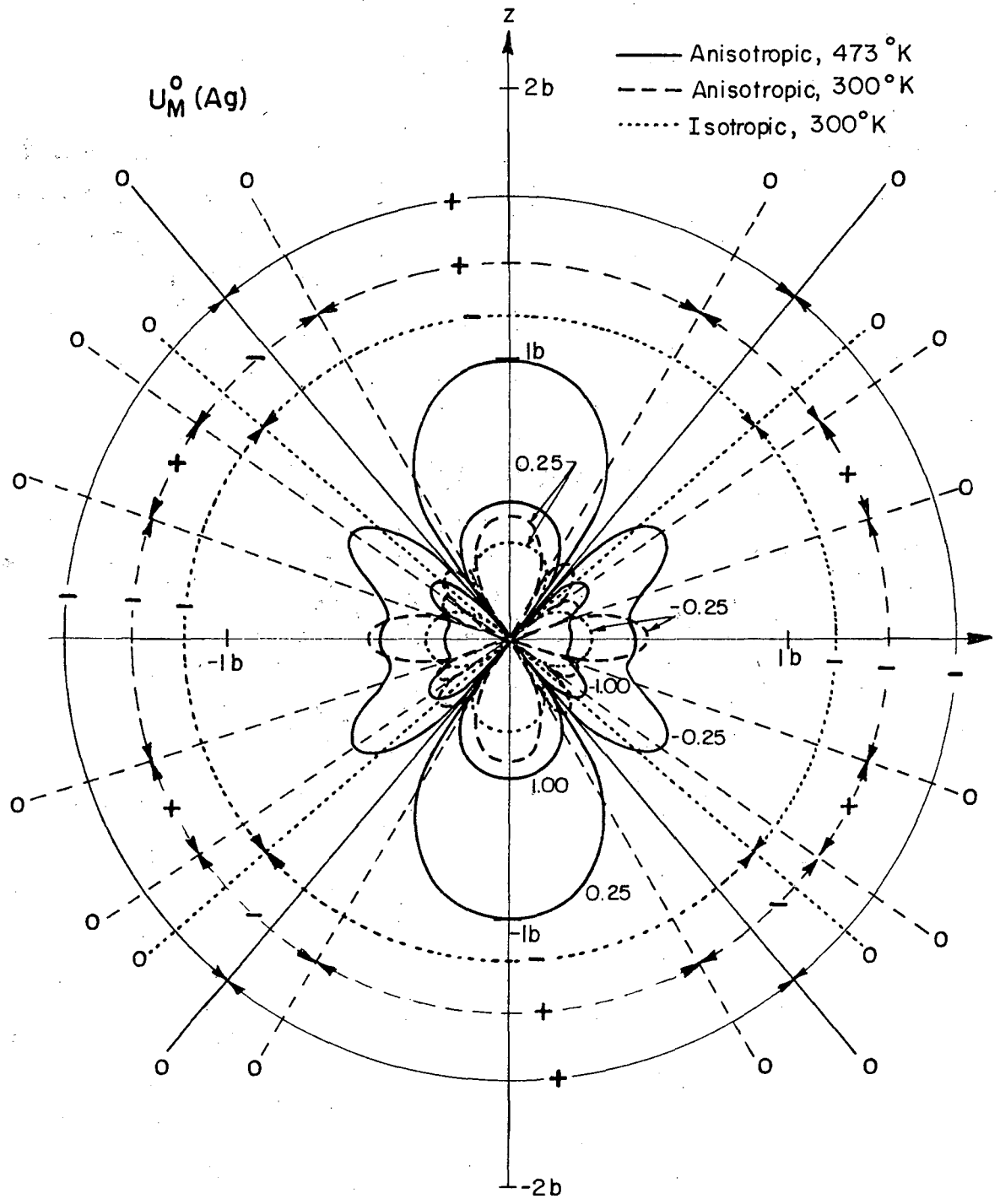

XBL 7310-5531

Fig. 4 (a)

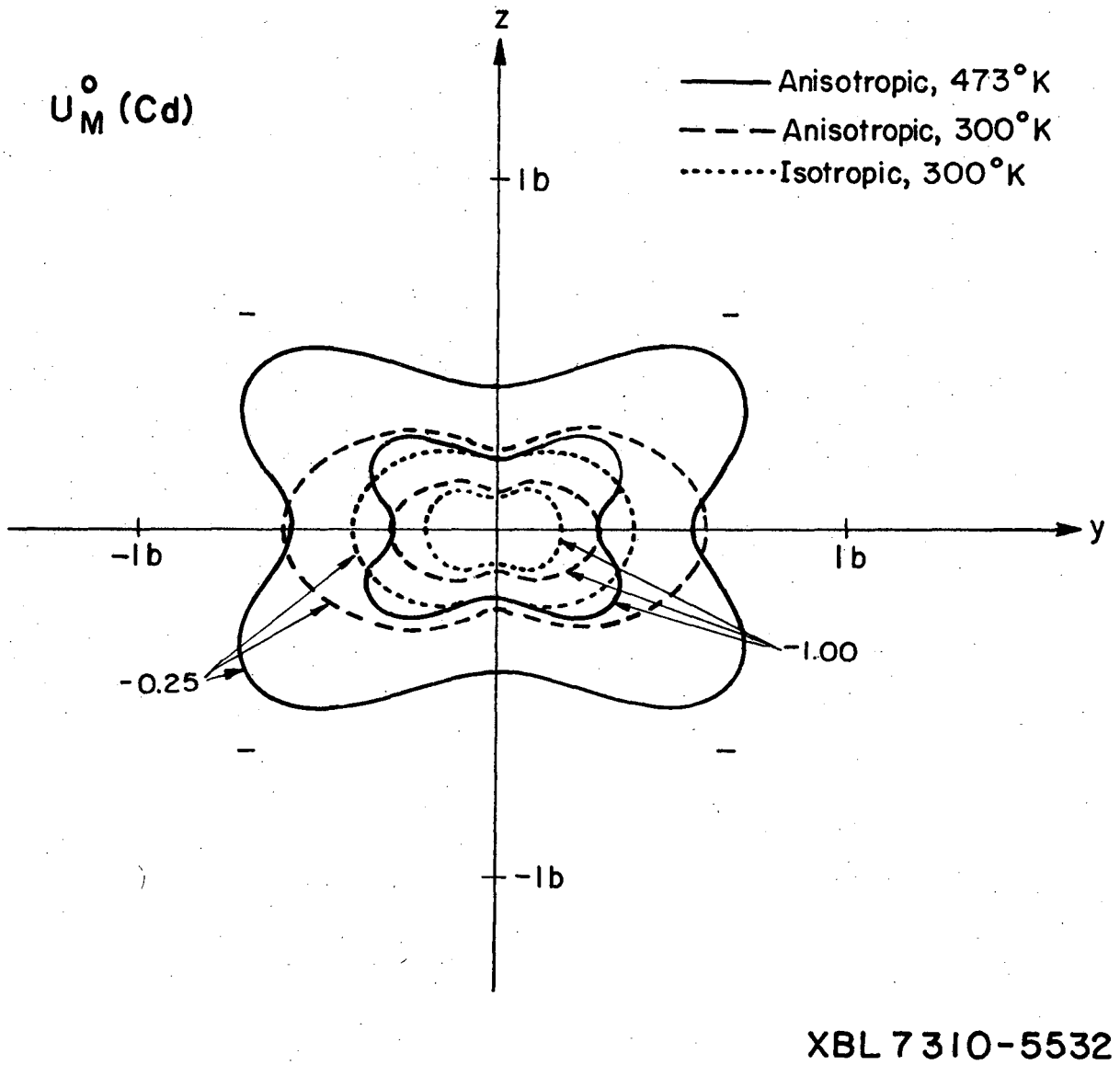
U_M^o (Cd)
Anisotropic, 473°K
Anisotropic, 300°K
Isotropic, 300°K
z
y
1b
-1b
-1b
1b
-0.25
-1.00
XBL 7310-5532

Fig. 4(b)

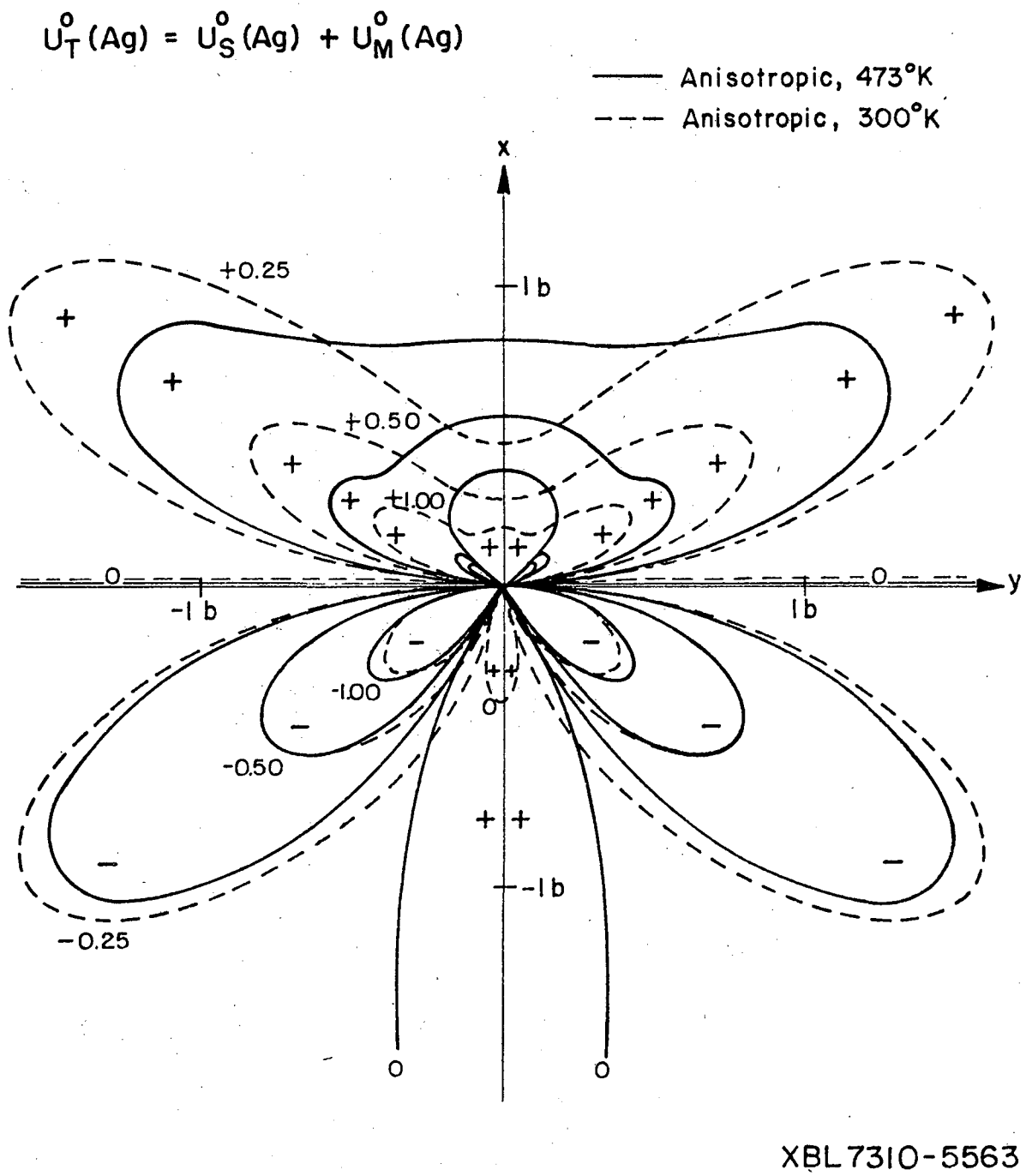
$U_T^o(Ag) = U_S^o(Ag) + U_M^o(Ag)$
Anisotropic, 473°K
Anisotropic, 300°K
x
y
+0.25
+0.50
+1.00
-1.00
-0.50
-0.25
1 b
-1 b
0
XBL 7310-5563

Fig. 5(a)

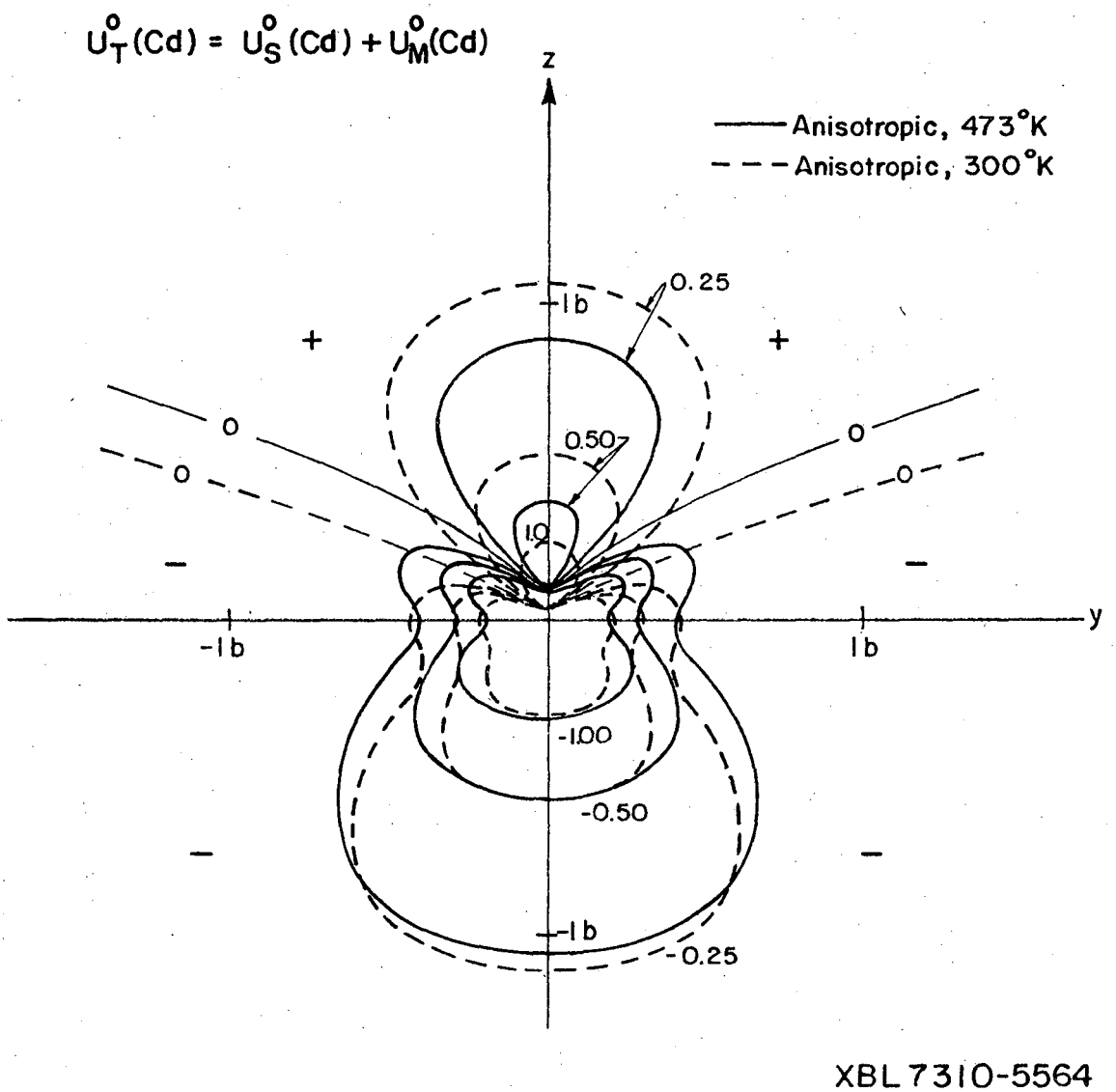
$U_T^o(Cd) = U_S^o(Cd) + U_M^o(Cd)$
z
Anisotropic, 473°K
Anisotropic, 300°K
0.25
1b
+
+
0
0
0
0
0.50
1.0
−
−
y
-1b
1b
-1.00
-0.50
−
−
-1b
-0.25
XBL 7310-5564

Fig. 5(b)

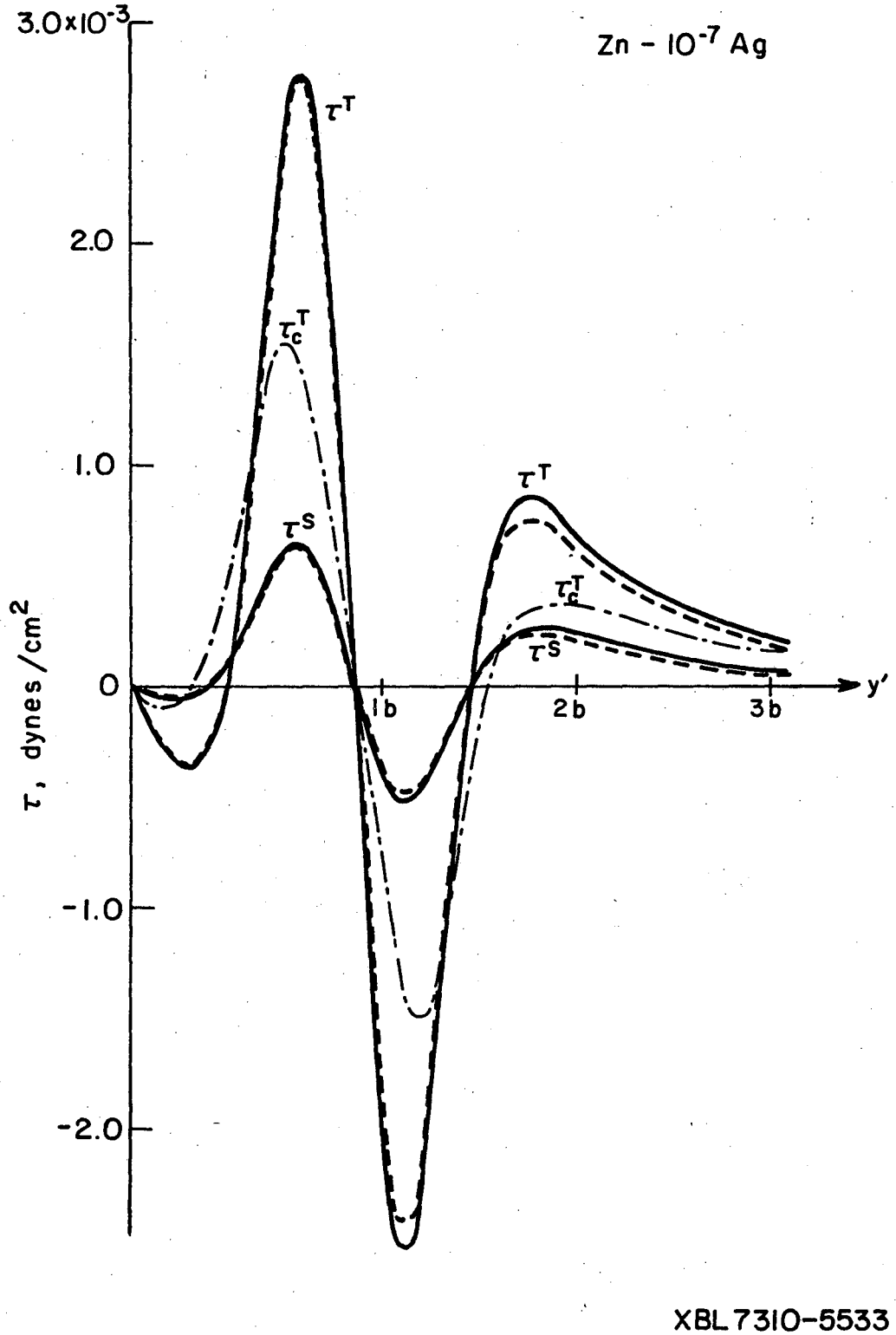
3.0×10⁻³
2.0
1.0
0
-1.0
-2.0
τ, dynes/cm²
Zn - 10⁻⁷ Ag
τ^T
τ_c^T
τ^S
τ^T
τ_c^T
τ^S
1b
2b
3b
y'
XBL 7310-5533

Fig. 6

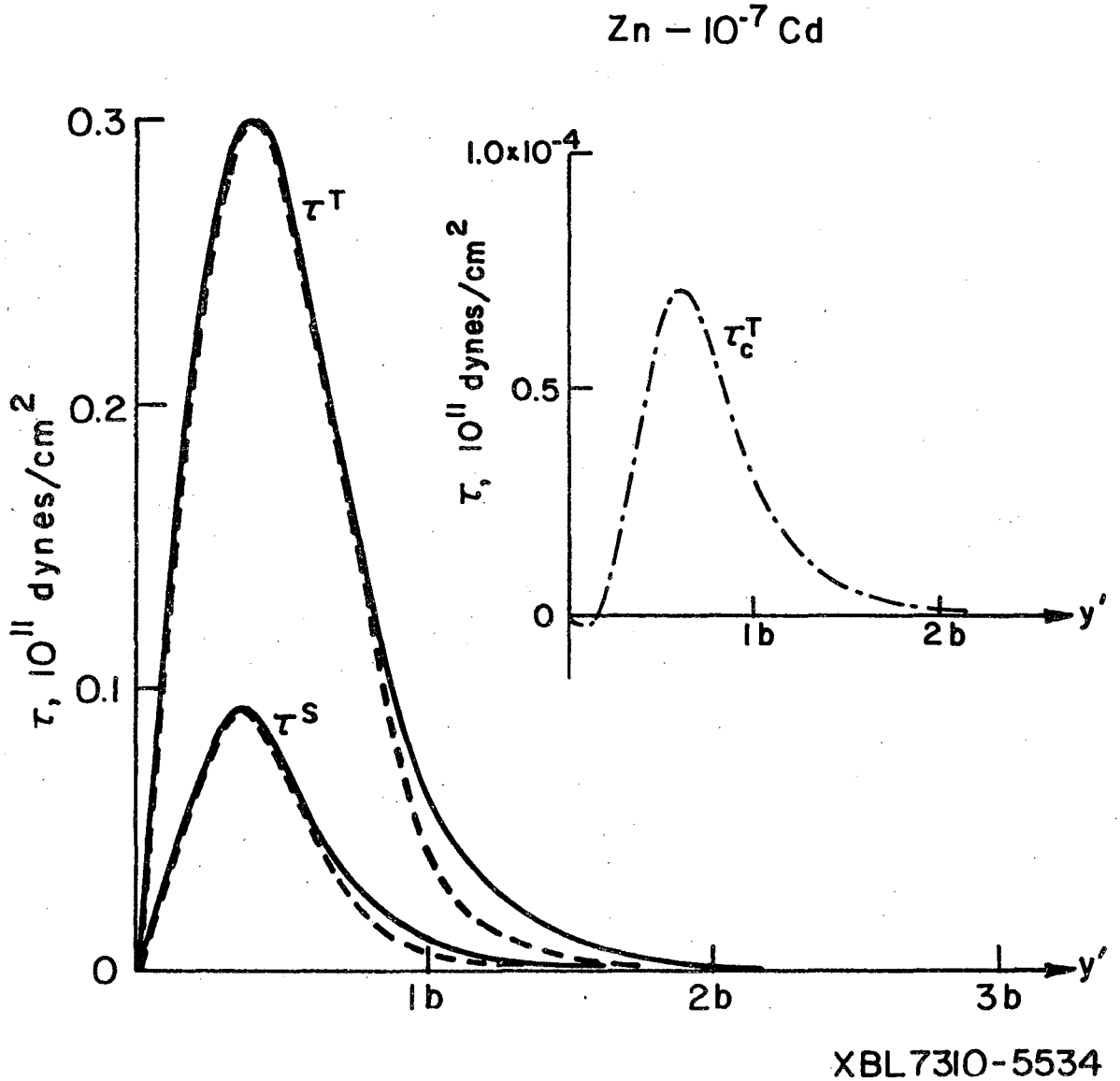
Zn – 10^-7 Cd
0.3
0.2
0.1
0
τ, 10^11 dynes/cm^2
τ^T
τ^S
1b
2b
3b
y'
1.0x10^-4
0.5
0
τ, 10^11 dynes/cm^2
τ_c^T
1b
2b
y'
XBL7310-5534

Fig. 7

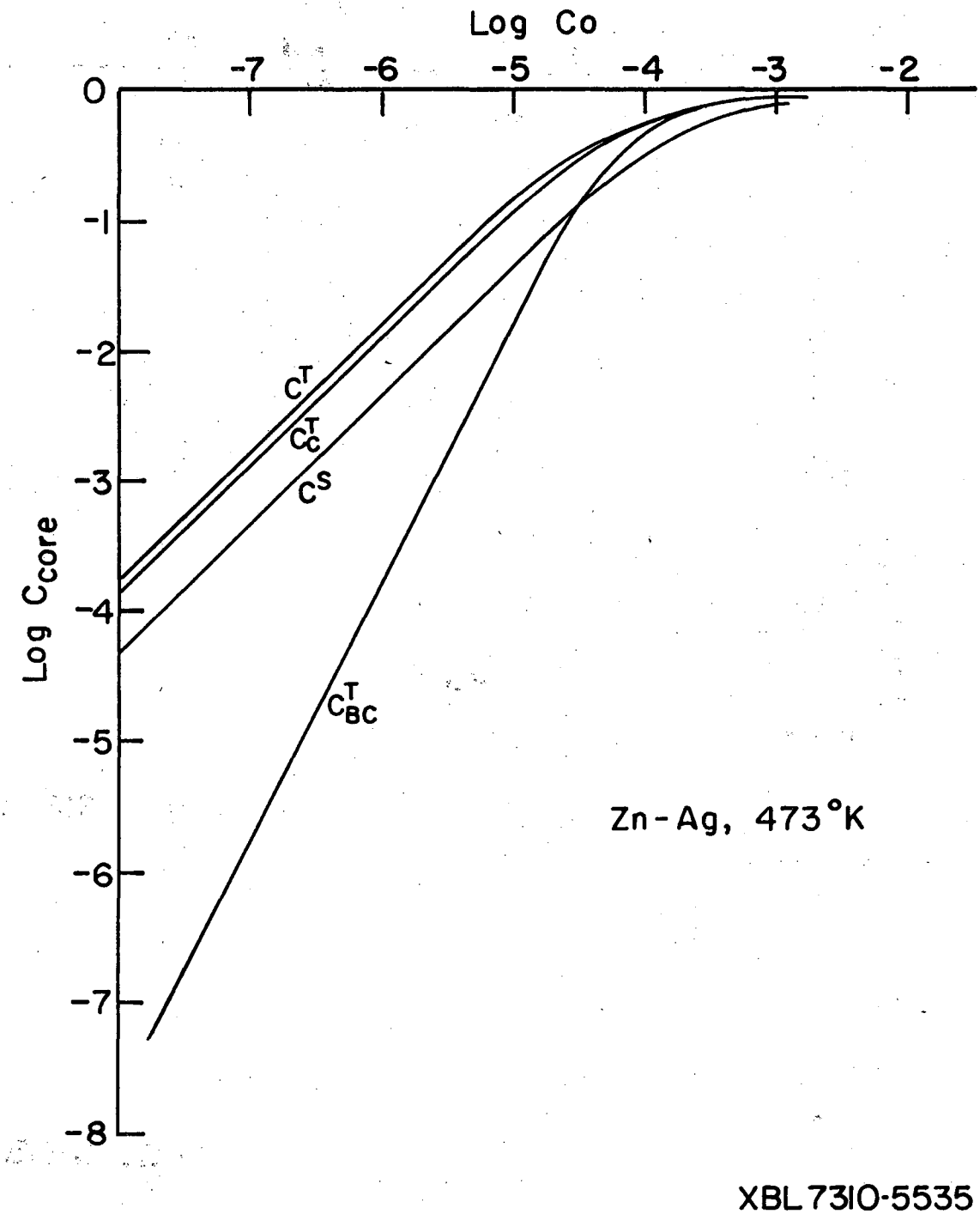

XBL 7310-5535

Fig. 8

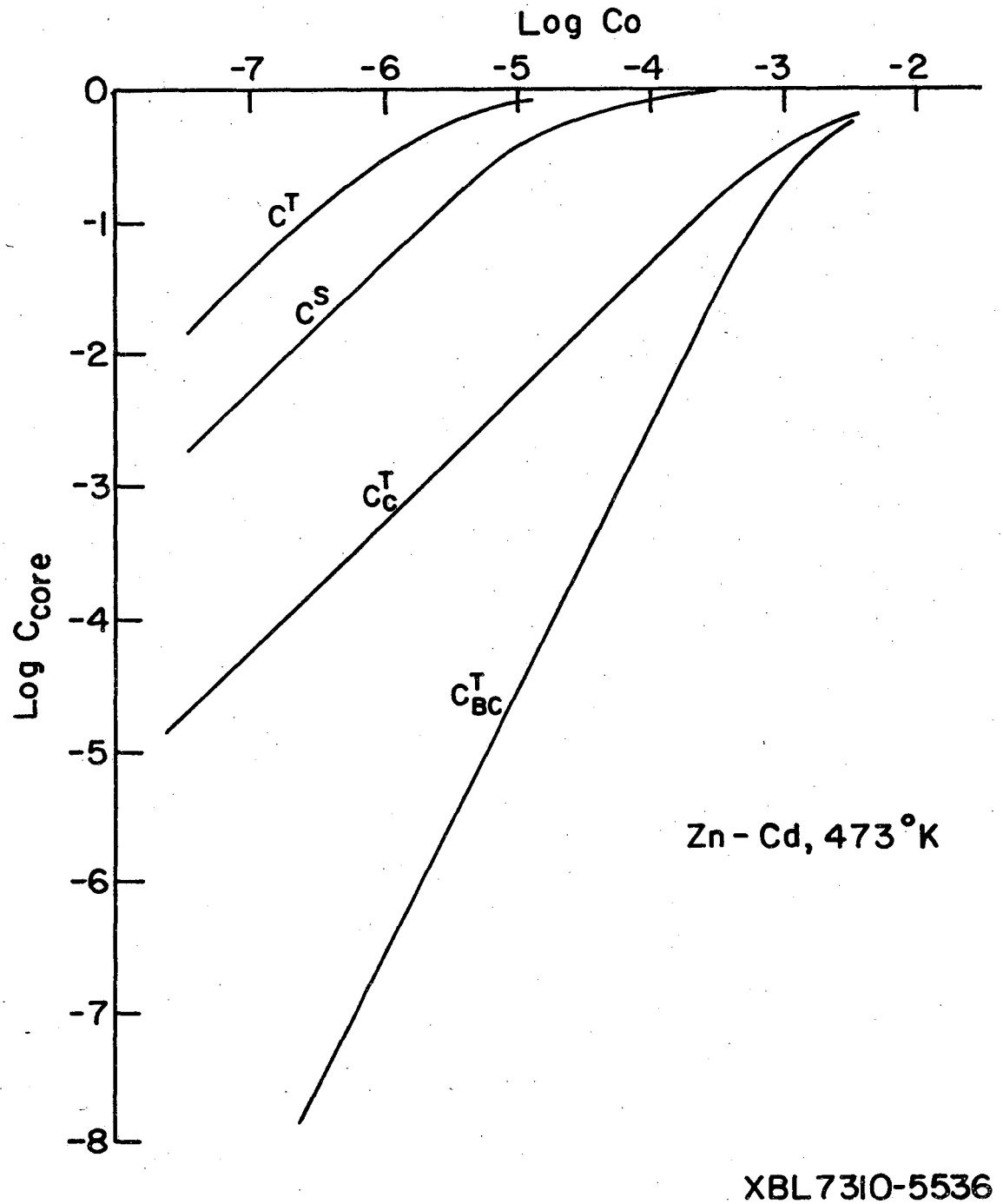
Log Co
-7
-6
-5
-4
-3
-2
0
-1
-2
-3
-4
-5
-6
-7
-8
Log C_{core}
C^T
C^S
C_C^T
C_{BC}^T
Zn - Cd, 473°K
XBL7310-5536

Fig. 9

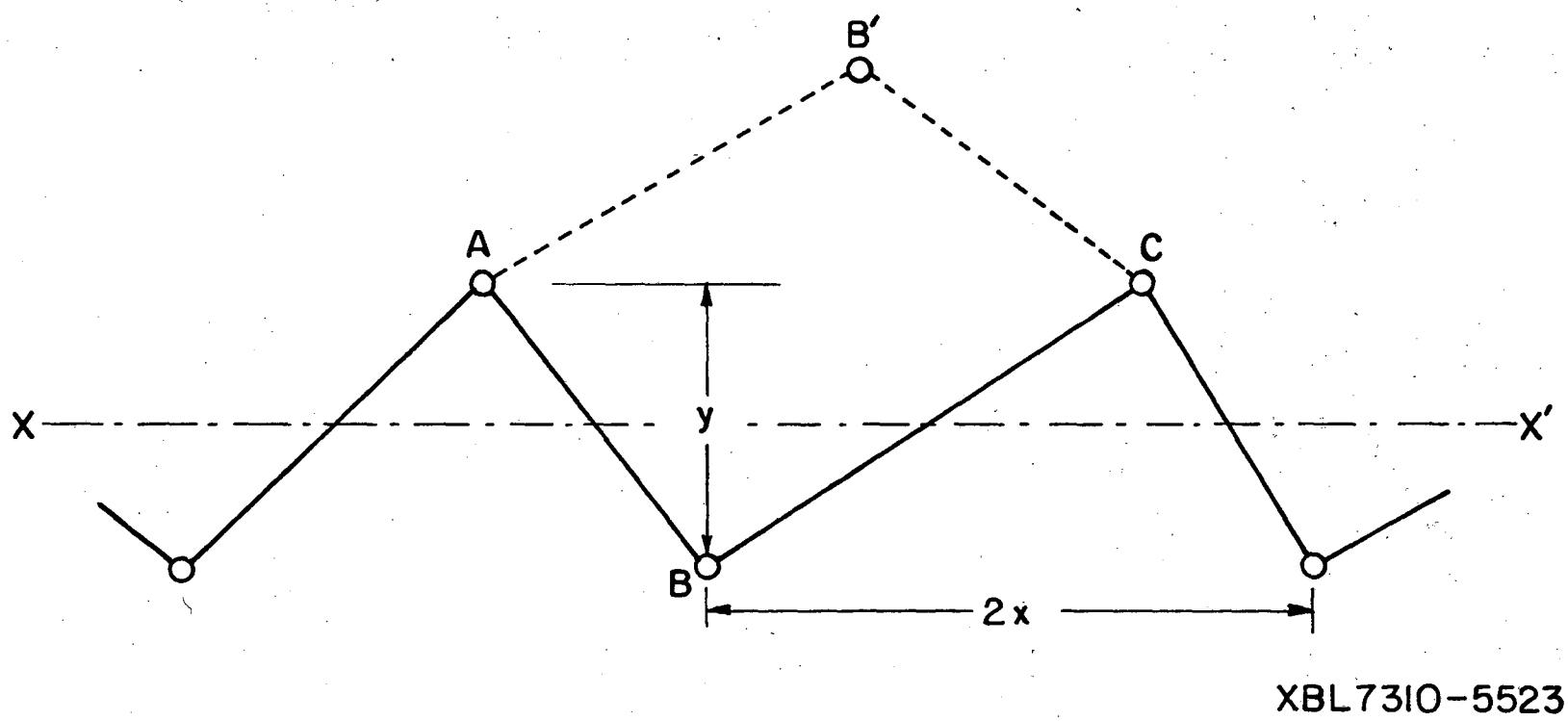

Fig. 10

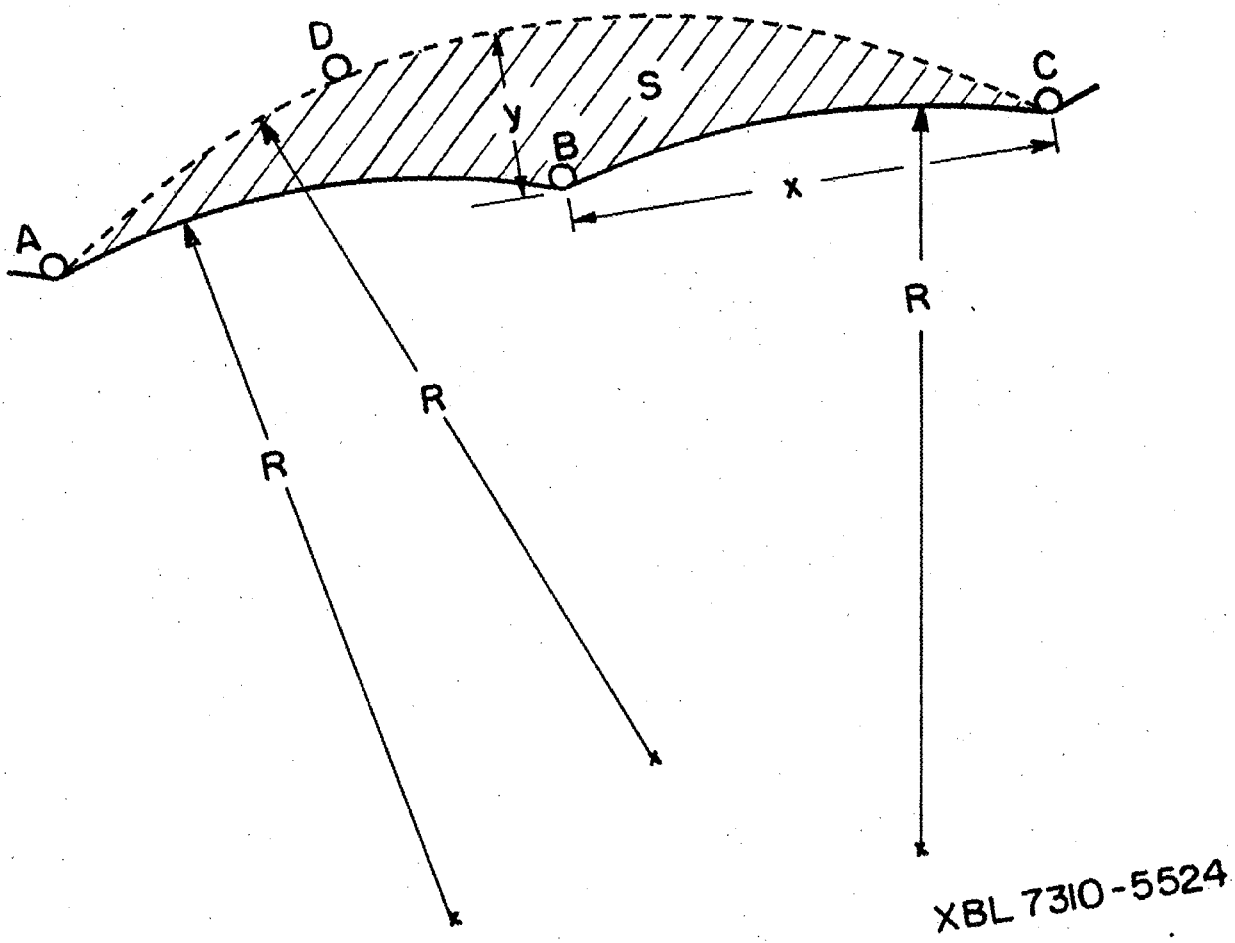

Fig. 11

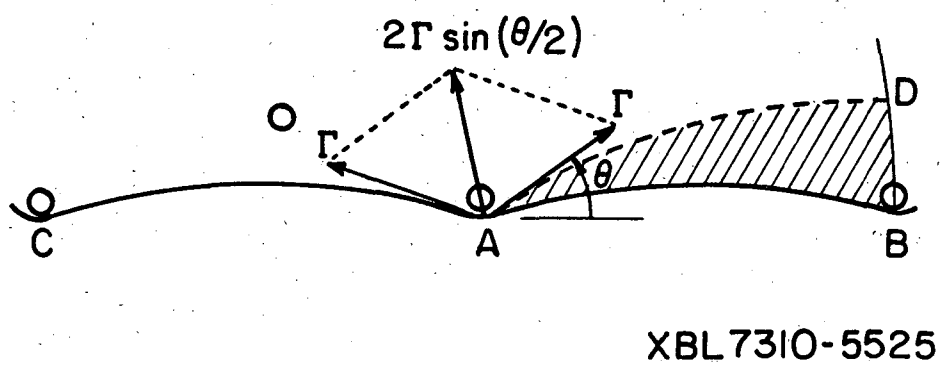

Fig. 12

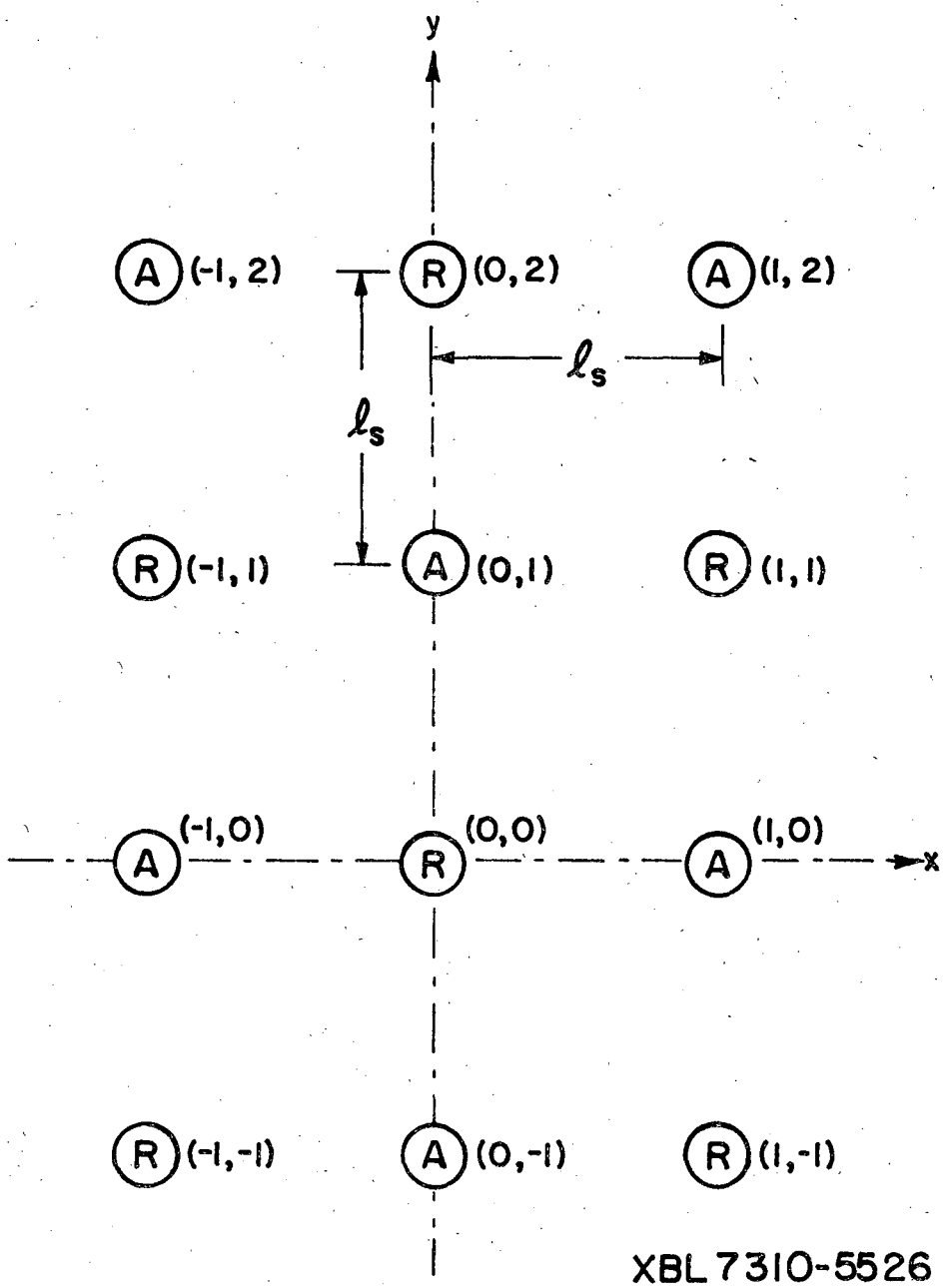
y
A (-1, 2)
R (0, 2)
A (1, 2)
ℓ_s
ℓ_s
R (-1, 1)
A (0, 1)
R (1, 1)
A (-1, 0)
R (0, 0)
A (1, 0)
x
R (-1, -1)
A (0, -1)
R (1, -1)
XBL 7310-5526

Fig. 13

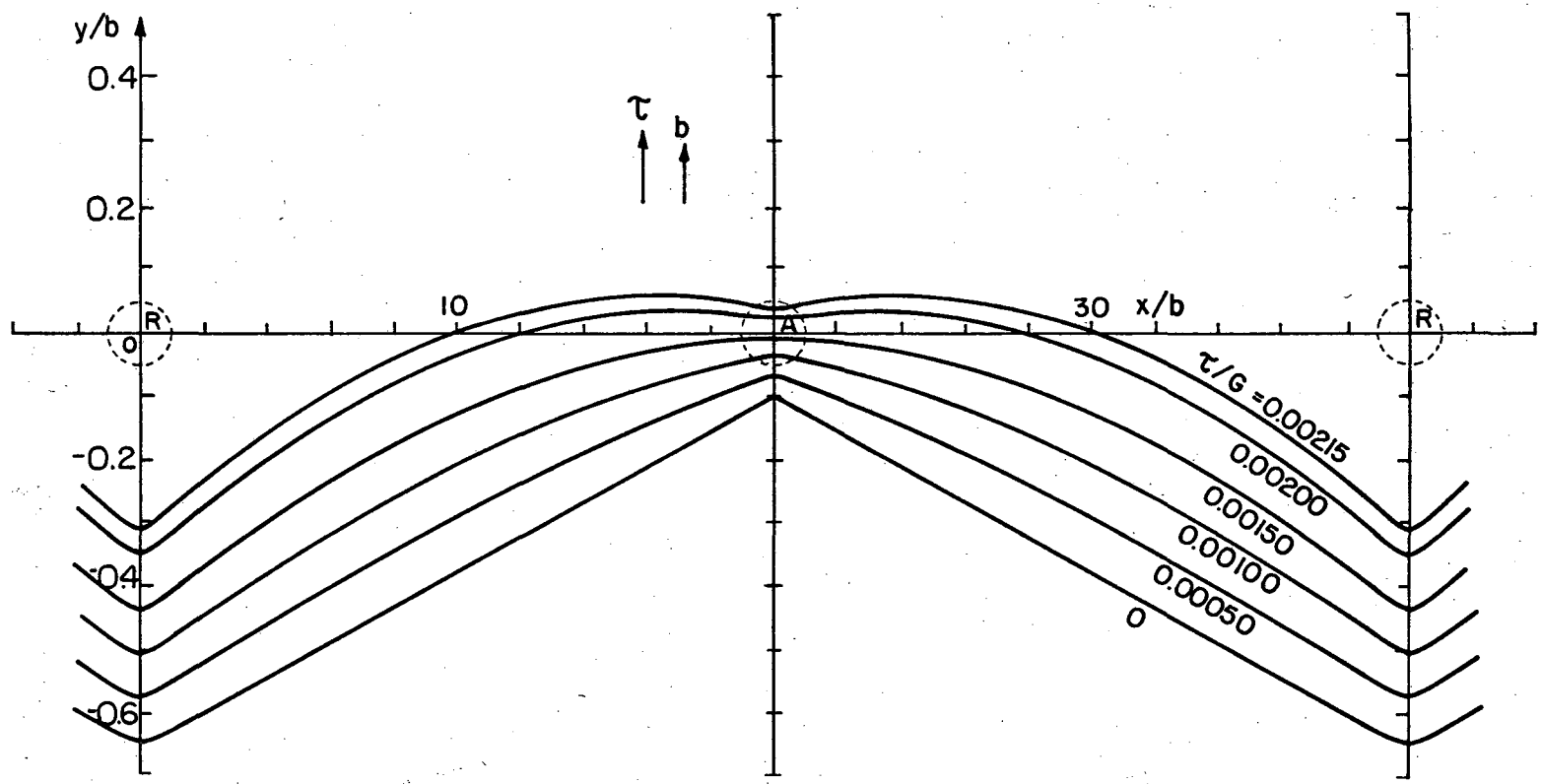

XBL 7310-5515

Fig. 14

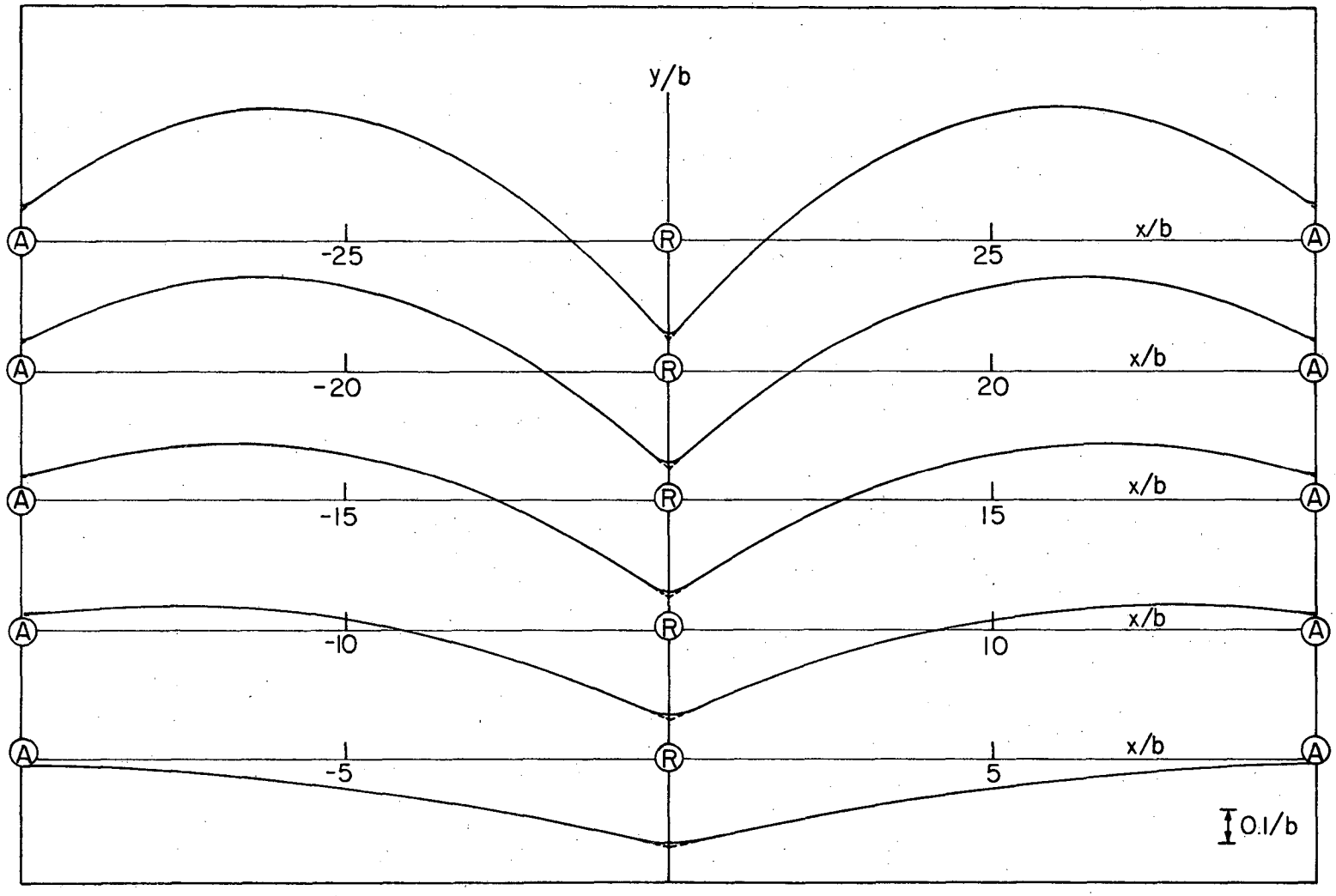

XBL 739 - 1874

Fig. 15

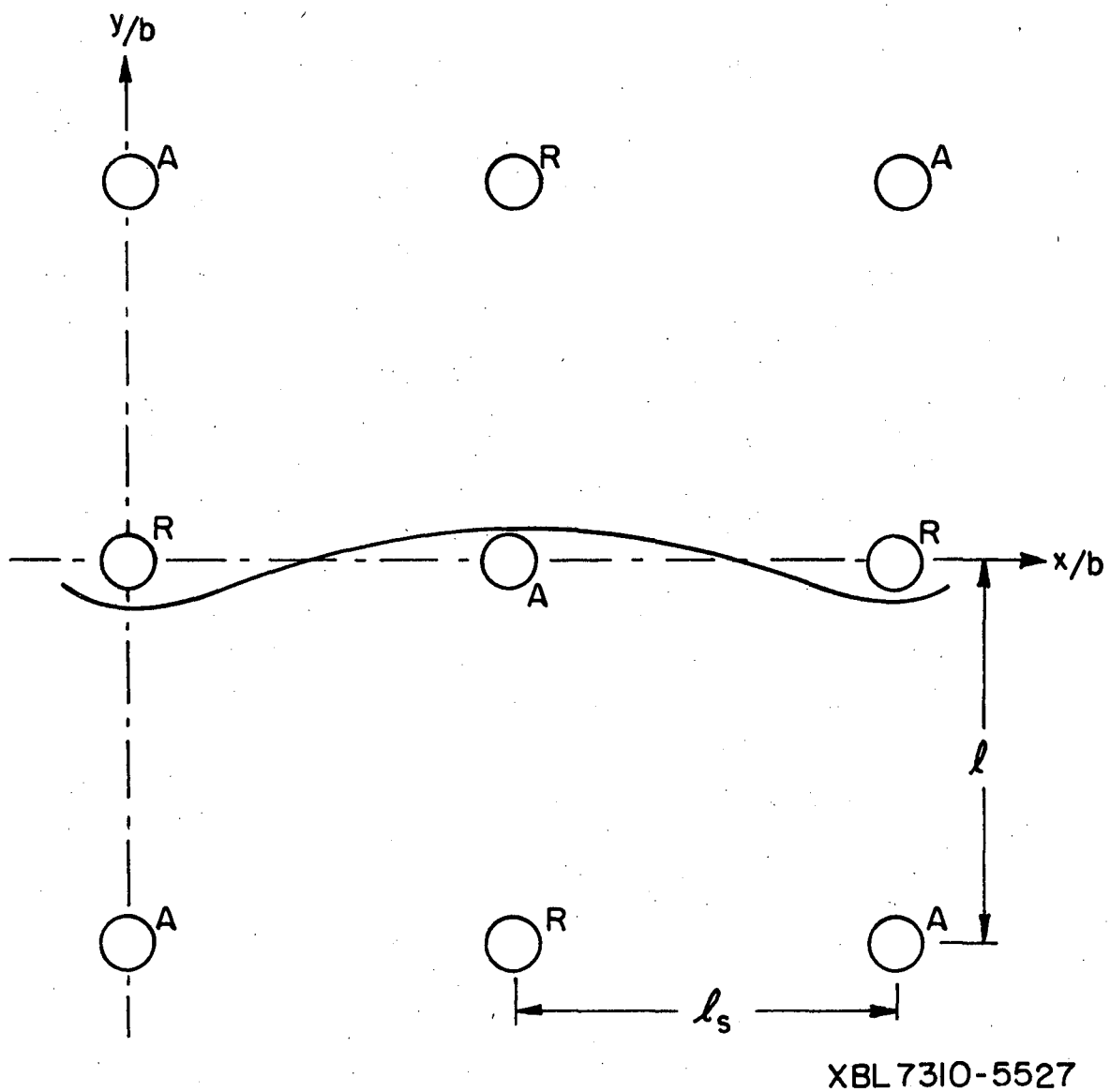

Fig. 16

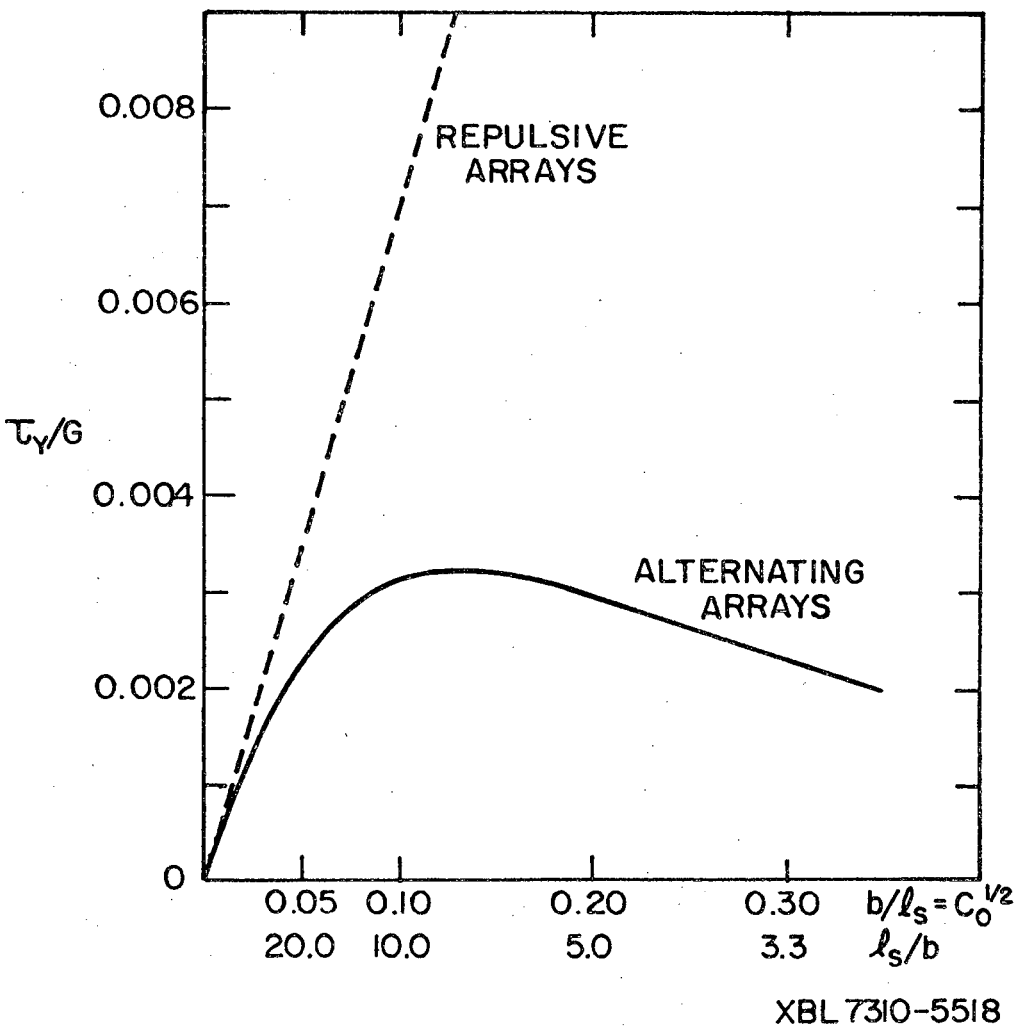
0.008
0.006
0.004
0.002
0
τ_Y/G
REPULSIVE ARRAYS
ALTERNATING ARRAYS
0.05 0.10 0.20 0.30 $b/\ell_s = C_o^{1/2}$
20.0 10.0 5.0 3.3 ℓ_s/b
XBL 7310-5518

Fig. 17

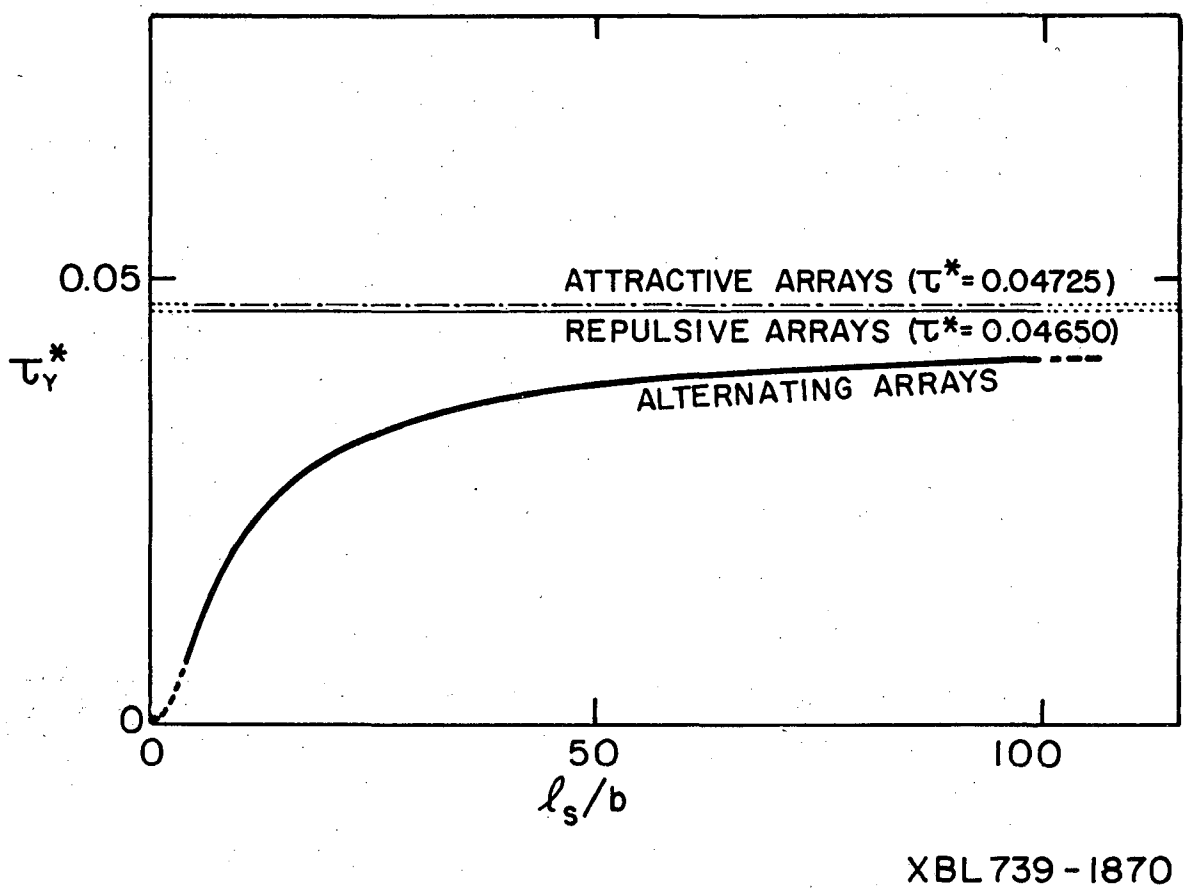
0.05
ATTRACTIVE ARRAYS (τ^*= 0.04725)
REPULSIVE ARRAYS (τ^*= 0.04650)
τ_Y^*
ALTERNATING ARRAYS
0
0
50
100
ℓ_s/b
XBL 739-1870

Fig. 18

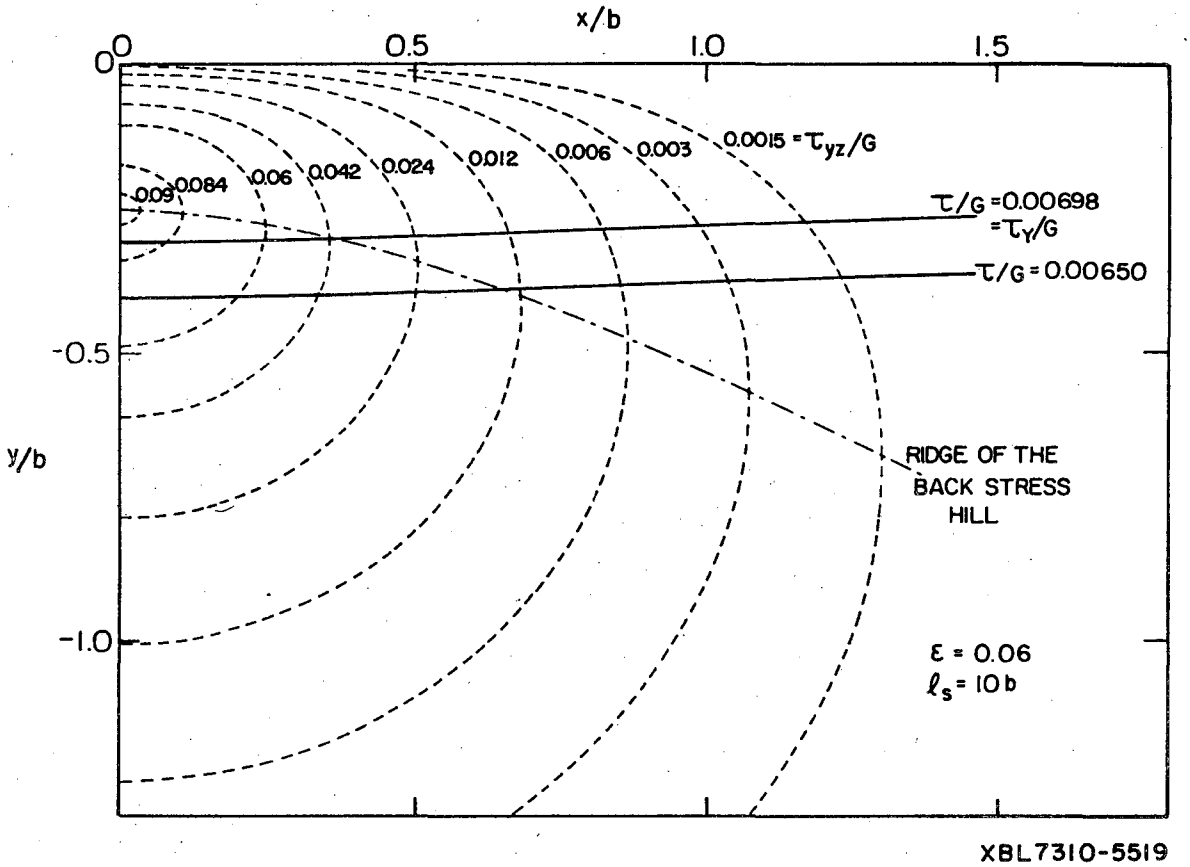
x/b
0
0.5
1.0
1.5
y/b
0
-0.5
-1.0
0.09
0.084
0.06
0.042
0.024
0.012
0.006
0.003
0.0015 = τyz/G
τ/G = 0.00698
= τY/G
τ/G = 0.00650
RIDGE OF THE
BACK STRESS
HILL
ε = 0.06
ℓs = 10 b
XBL7310-5519

Fig. 19(a)

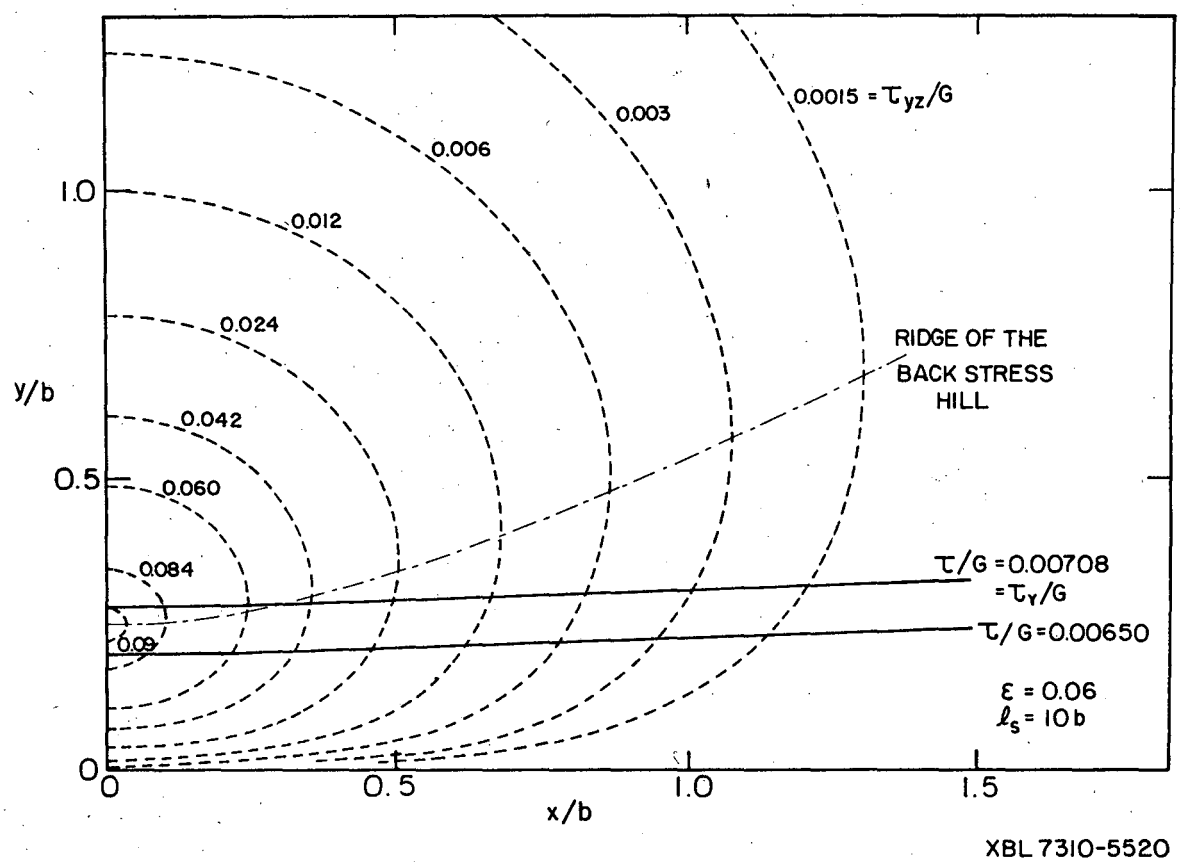
0.0015 = τ_{yz}/G
0.003
0.006
0.012
0.024
0.042
0.060
0.084
0.09
RIDGE OF THE
BACK STRESS
HILL
$\tau/G = 0.00708$
$= \tau_Y/G$
$\tau/G = 0.00650$
$\varepsilon = 0.06$
$\ell_s = 10b$
y/b
x/b
0
0.5
1.0
1.5
XBL 7310-5520

Fig. 19(b)

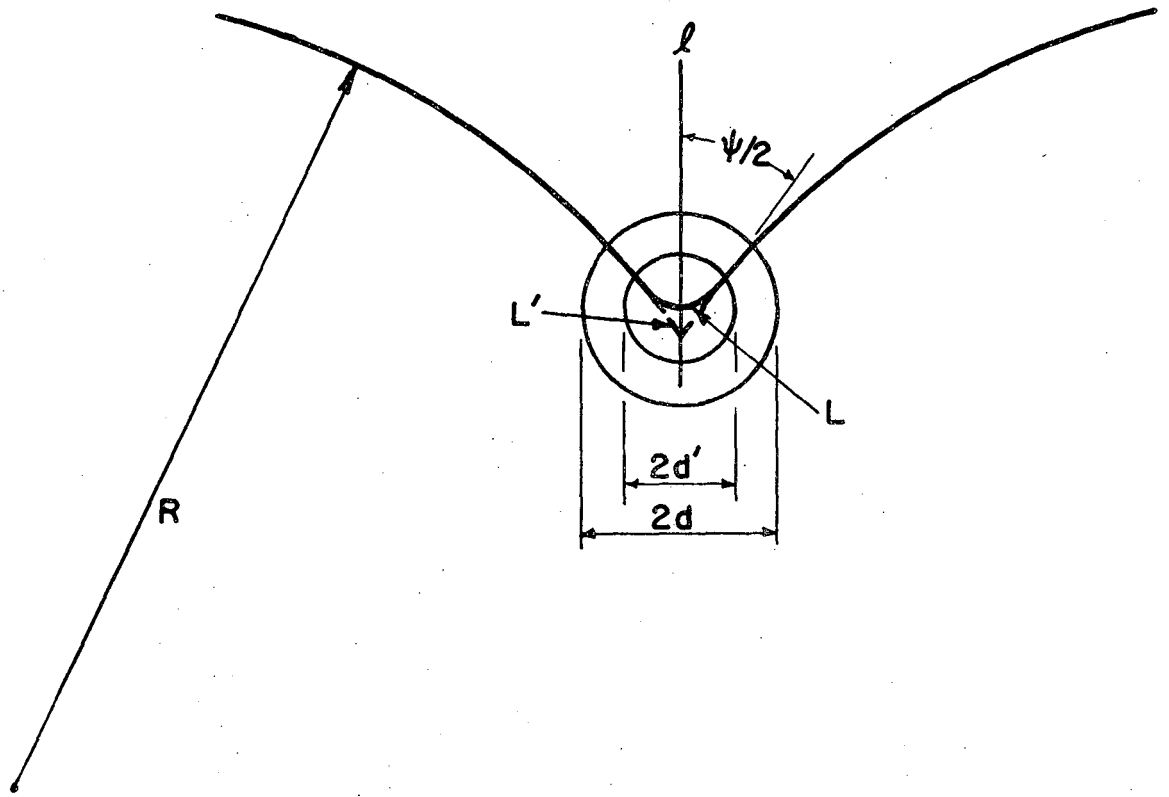

XBL732-5723

Fig. 20

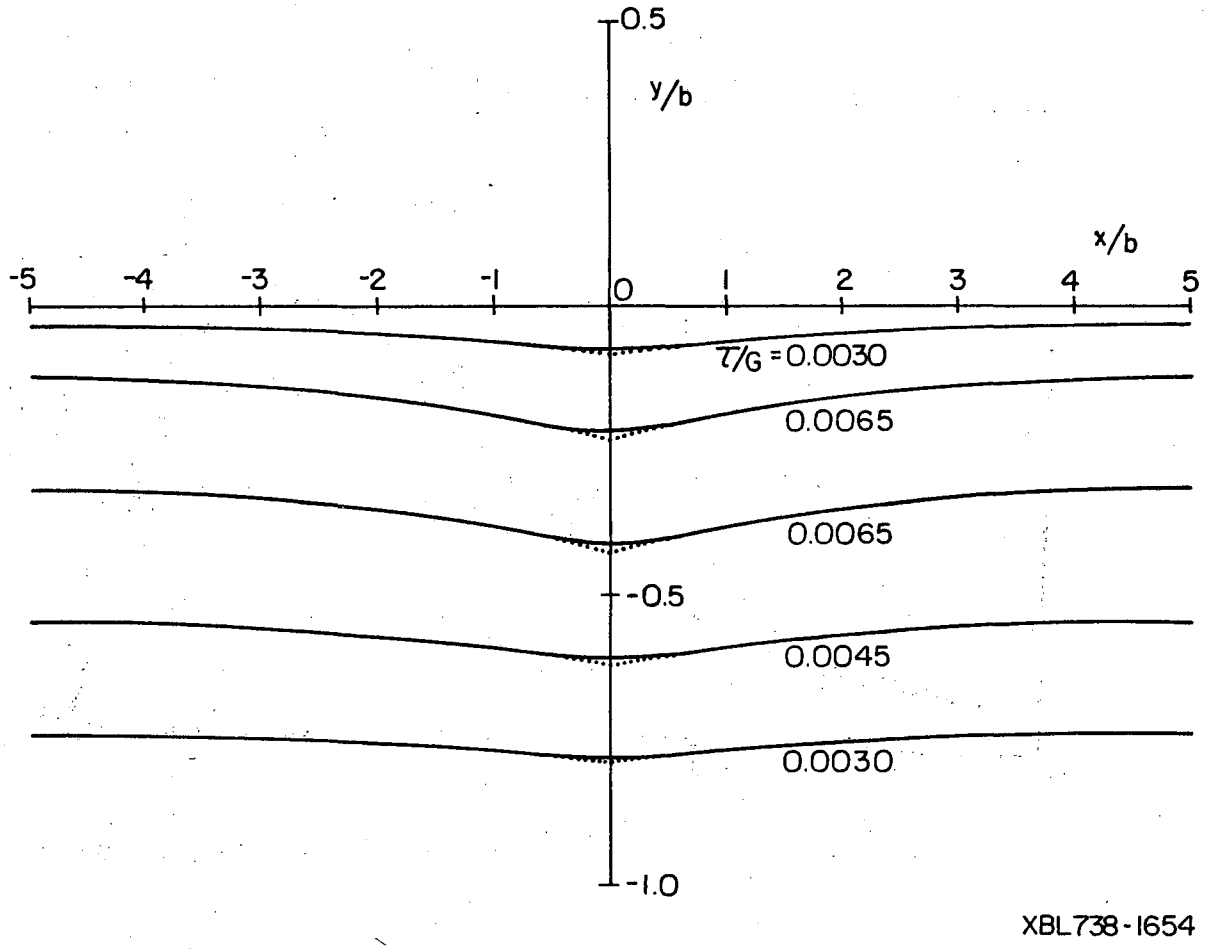
0.5
y/b
x/b
-5
-4
-3
-2
-1
0
1
2
3
4
5
τ/G = 0.0030
0.0065
0.0065
-0.5
0.0045
0.0030
-1.0
XBL738-1654

Fig. 21

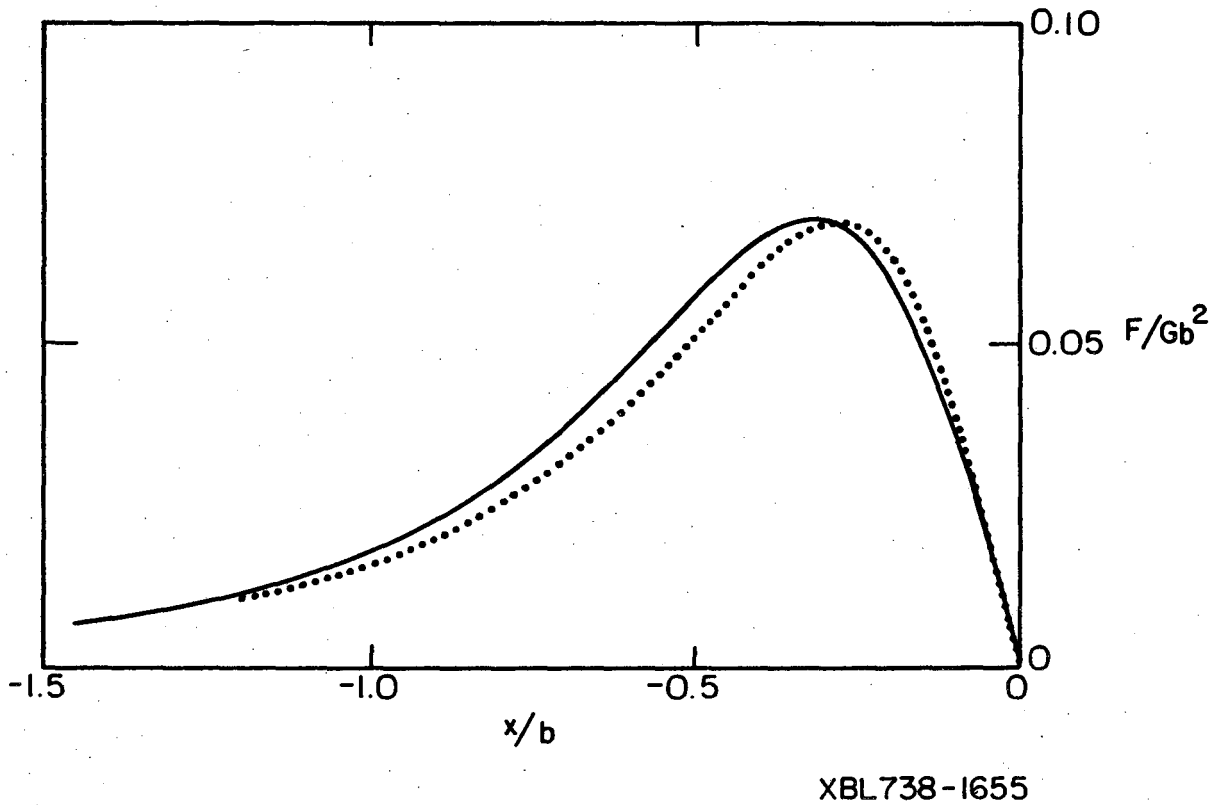

Fig. 22(a)

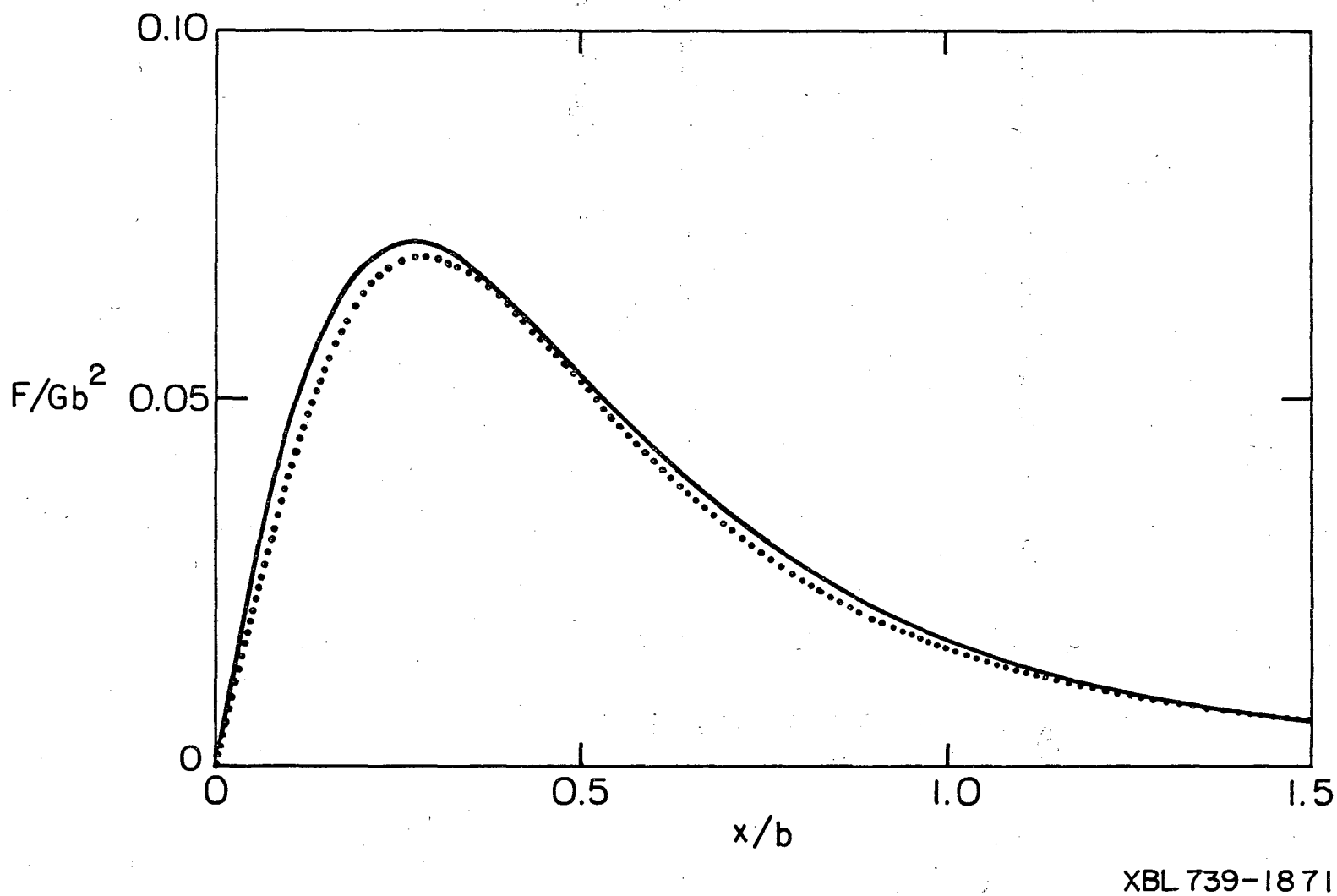

Fig. 22(b)

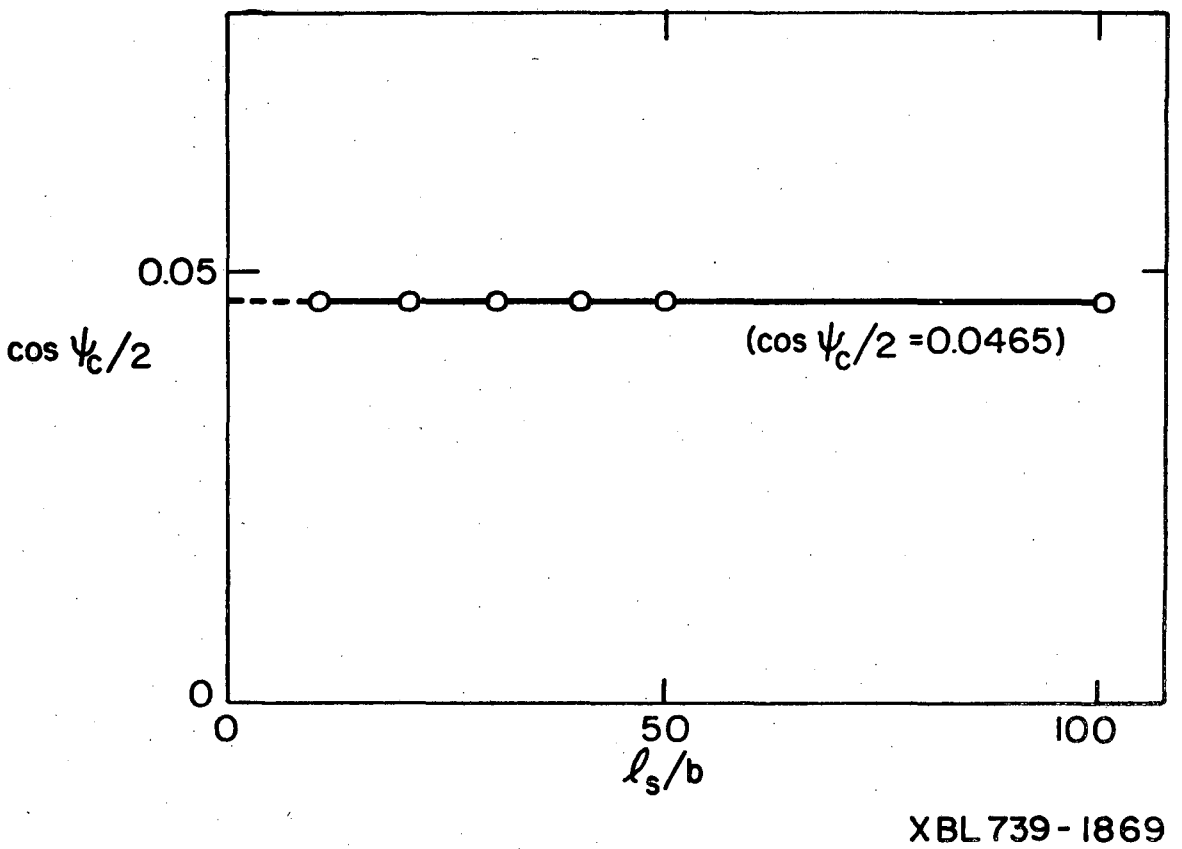

Fig. 23

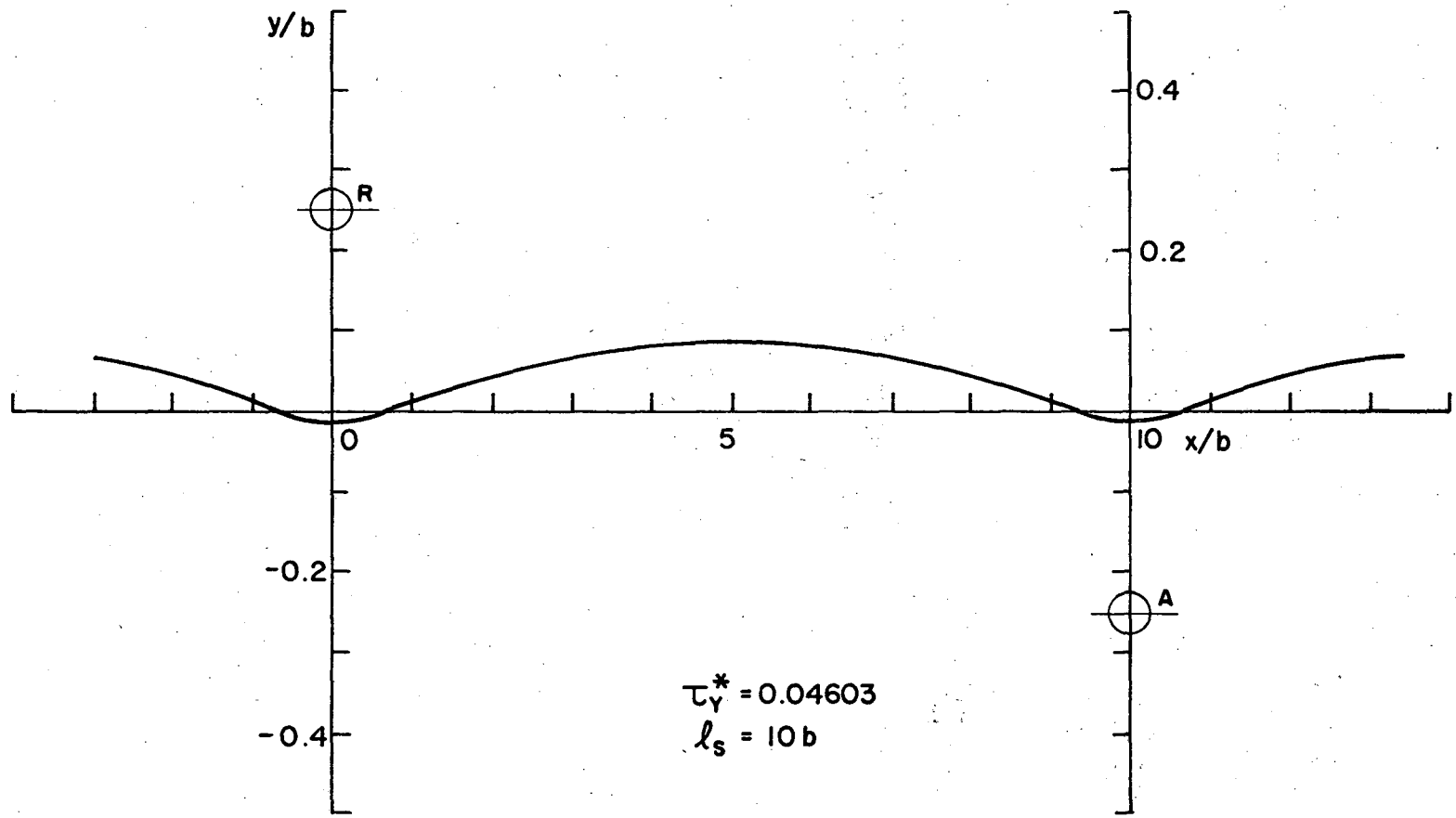

XBL 7310-5521

Fig. 24

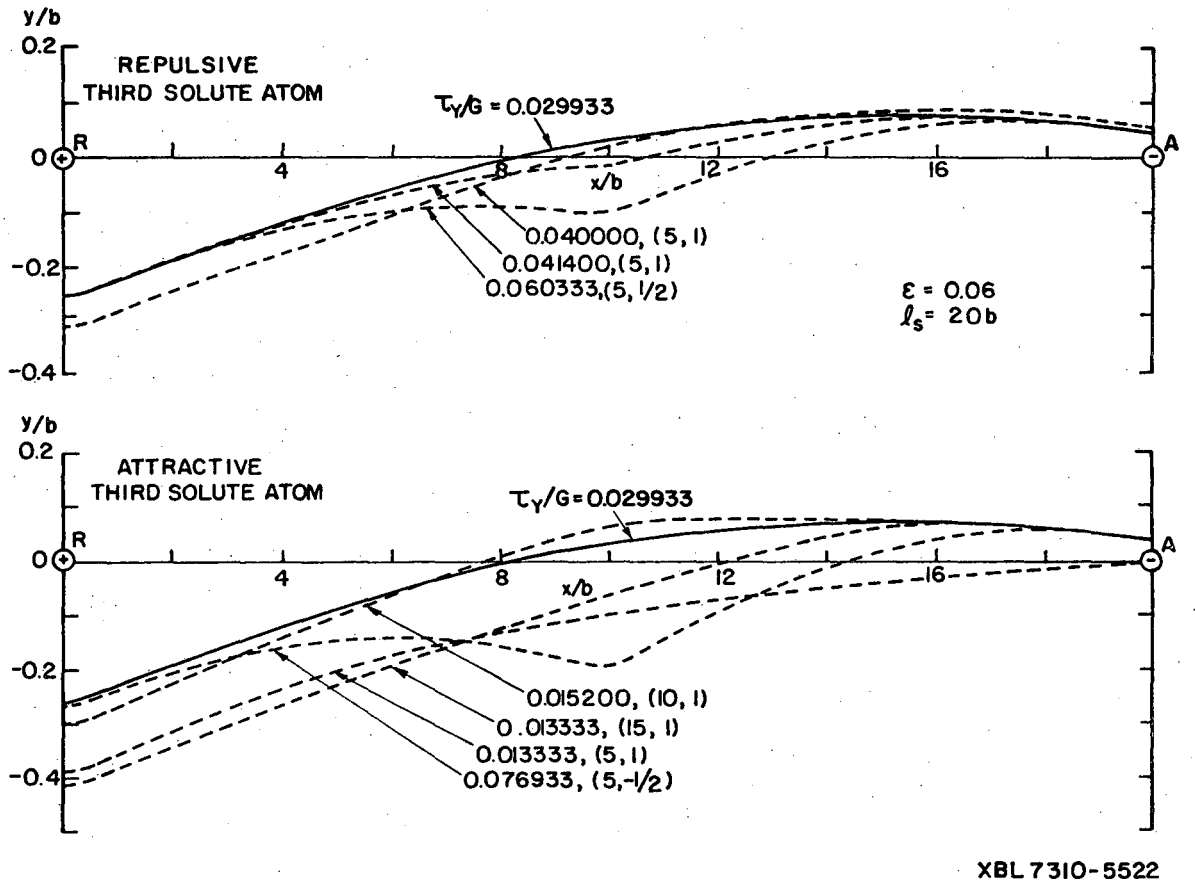
y/b
0.2
REPULSIVE
THIRD SOLUTE ATOM
τ_Y/G = 0.029933
0
R
4
8
x/b
12
16
A
0.040000, (5, 1)
0.041400,(5, 1)
0.060333,(5, 1/2)
-0.2
ε = 0.06
ℓ_s = 20b
-0.4
y/b
0.2
ATTRACTIVE
THIRD SOLUTE ATOM
τ_Y/G=0.029933
0
R
4
8
x/b
12
16
A
-0.2
0.015200, (10, 1)
0.013333, (15, 1)
0.013333, (5, 1)
0.076933, (5,-1/2)
-0.4
XBL 7310-5522

Fig. 25

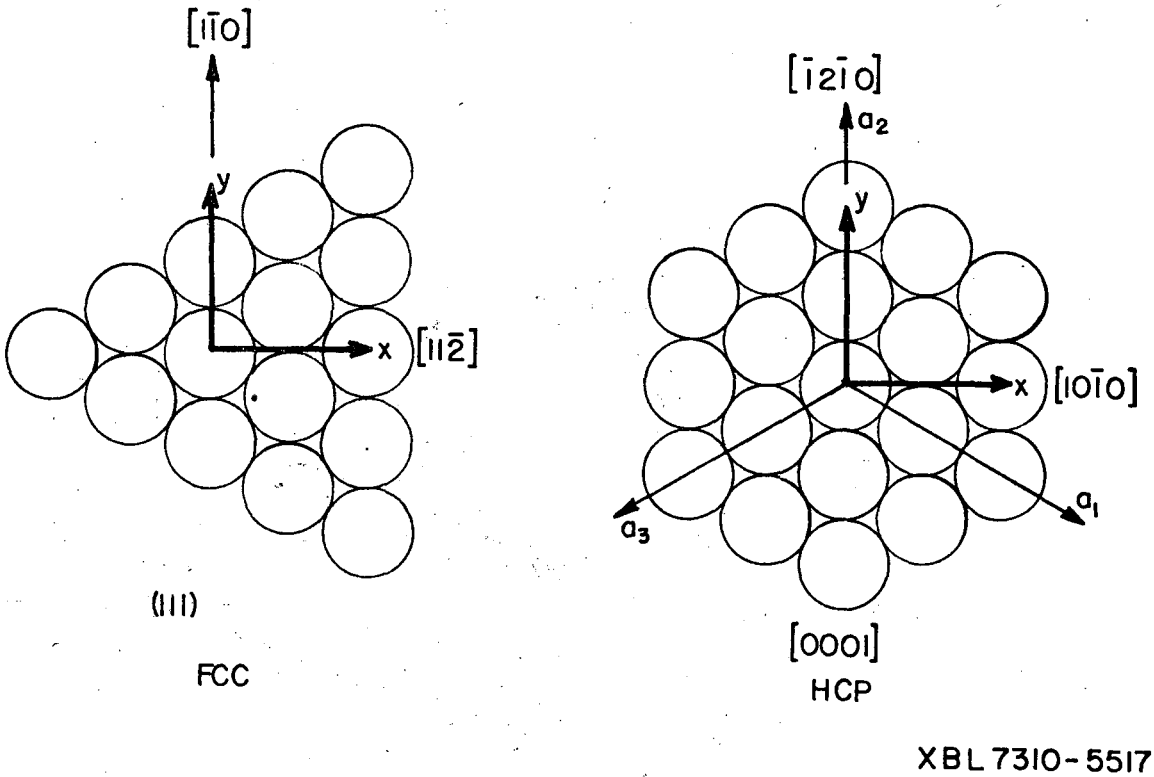
[1$\bar{1}$0]
y
x
[11$\bar{2}$]
(111)
FCC
[$\bar{1}$2$\bar{1}$0]
a_2
y
x
[10$\bar{1}$0]
a_1
a_3
[0001]
HCP
XBL 7310-5517

Fig. A1

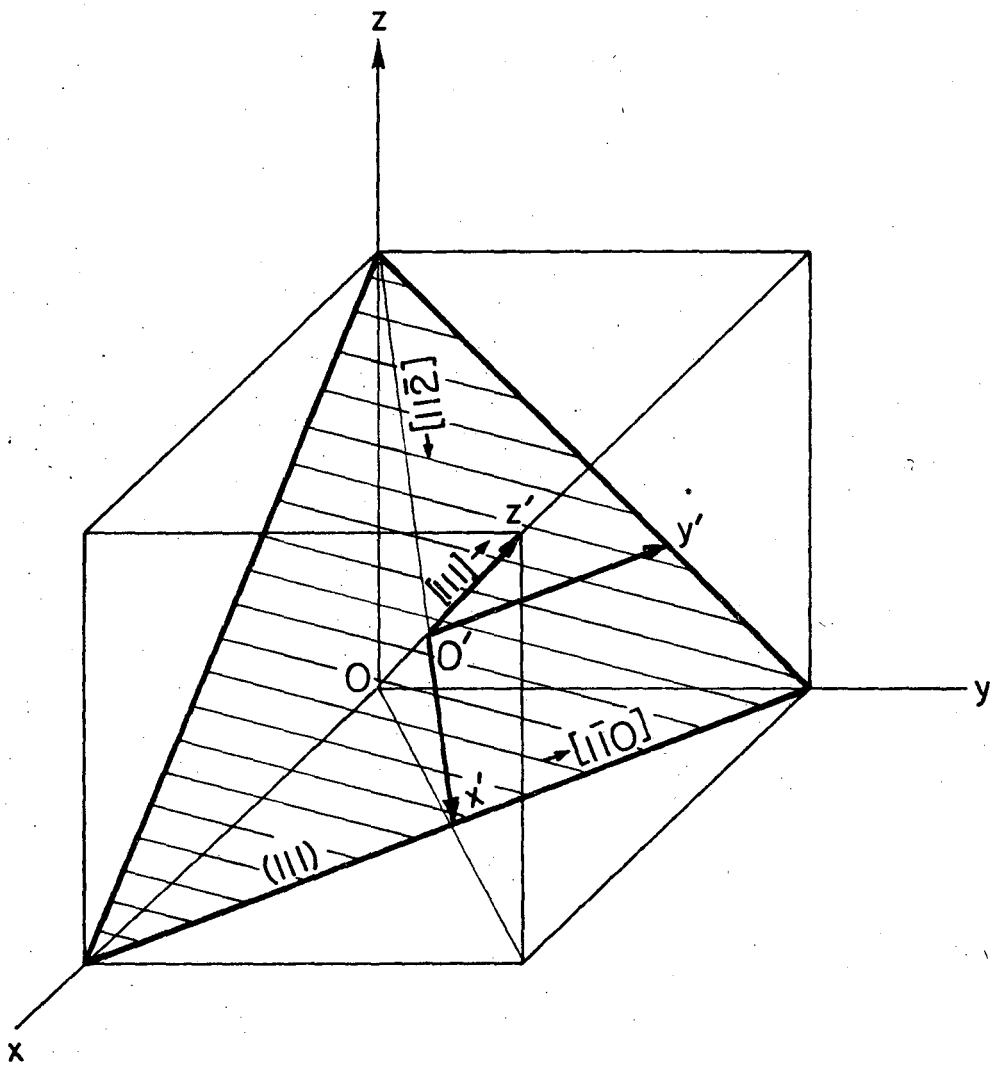

XBL 7310-5516

Fig. A2

LEGAL NOTICE

This report was prepared as an account of work sponsored by the United States Government. Neither the United States nor the United States Atomic Energy Commission, nor any of their employees, nor any of their contractors, subcontractors, or their employees, makes any warranty, express or implied, or assumes any legal liability or responsibility for the accuracy, completeness or usefulness of any information, apparatus, product or process disclosed, or represents that its use would not infringe privately owned rights.

TECHNICAL INFORMATION DIVISION
LAWRENCE BERKELEY LABORATORY
UNIVERSITY OF CALIFORNIA
BERKELEY, CALIFORNIA 94720